Modeling of Silicon Photonic Device for WDM application and for Non-Reciprocal Optical Systems

by

Mirza Fuad Adnan

MASTER OF SCIENCE

IN

ELECTRICAL AND ELECTRONIC ENGINEERING

Department of Electrical and Electronic Engineering
Islamic University of Technology (IUT)
Board Bazar, Gazipur-1704, Bangladesh
March, 2019

CERTIFICATE OF APPROVAL

The thesis titled 'Modeling of Silicon Photonic Device for WDM application and for Non-Reciprocal Optical Systems' submitted by Mirza Fuad Adnan, St. No. 152616 of Academic year 2015-16 has been found as satisfactory and accepted as partial fulfillment of the requirement for the Degree MASTER OF SCIENCE IN ELECTRICAL AND ELECTRONIC ENGINEERING on March 11, 2019.

1.

Dr. Md. Ruhul Amin (Supervisor) — Chairman
Professor and Head,
Electrical and Electronic Engineering Department,
Islamic University of Technology (IUT), Gazipur.

2.

Head, — Ex-Officio
Electrical and Electronic Engineering Department,
Islamic University of Technology (IUT), Gazipur.

3.

Dr. Md. Ashraful Hoque — Member
Professor,
Electrical and Electronic Engineering Department,
Islamic University of Technology (IUT), Gazipur.

4.

Dr. Mohammad Rakibul Islam — Member
Professor,
Electrical and Electronic Engineering Department,
Islamic University of Technology (IUT), Gazipur.

5.

Dr. Md. Shah Alam — Member (External)
Professor,
Electrical and Electronic Engineering Department,
Bangladesh University of Engineering and Technology (BUET),
Dhaka.

Declaration of Candidate

It is hereby declared that this thesis report or any part of it has not been submitted elsewhere for the award of any Degree or Diploma.

_____	_____
Dr. Md. Ruhul Amin	Mirza Fuad Adnan
Professor and Head,	Student No.:152616
Electrical and Electronic Engineering Department,	Academic Year: 2015-16
Islamic University of Technology (IUT).	Date:
Date:	

Dedicated to my parents

Who

have the most influence on me.

Table of contents

List of Figures

List of Tables

List of Abbreviation of Technical Terms

SOI	Silicon On Insulator
ORR	Optical Ring Resonator
WDM	Wavelength Division Multiplexing
DWDM	Dense Wavelength Division Multiplexing
CWDM	Coarse Wavelength Division Multiplexing
LTI	Linear Time Invariant
LTV	Linear Time Variant
TE	Transverse Electric
TM	Transverse Magnetic
SW	Shallow Water

ACKNOWLEDGMENTS

First of all, I offer gratitude to the almighty Allah (SWT), the most merciful and beneficial, for giving me the capability to do this research with good health.

It is a great pleasure to express my deepest sense of gratitude to my research supervisor, Prof. Dr. Md. Ruhul Amin for his scholastic supervision and constructive guidance throughout the progress of this work. He created a very good research environment for which I was able to explore many ideas without constraints.

The Head of computer Center deserves special mention for his outstanding and generous helps in arranging the simulation tools of this work. I am very grateful to him for his important suggestions and cooperation during my research.

I also express my heartily gratitude to Mr. Pankaj Jha, Technical Personnel CST simulation software for his guidelines and Suggestions during my research.

I would like to thank all the faculty members of the department of EEE, IUT for their inspiration and help during the course of this work.

Finally, I would mention very special thanks to my parents, sister and friends for their moral support and inspiration throughout this research work. Without them it would never have been possible for me to make it this far

Mirza Fuad Adnan

March,2019

ABSTRACT

This dissertation is aimed at the integration of a novel Magnetless optical waveguide isolator on a Silicon-on-Insulator platform. Optical isolation and non-reciprocal transmission have been raising significant interest in recent research. Optical nonreciprocity is essential in WDM technology in order to avoid backscattering of light to any of the input ports. In this dissertation to design the optical isolator, a novel technique has been entreated. The technique exerts the concept of Tesla-type fluidic valve in Electromagnetics. A mathematical correspondence between the mechanical wave and Electromagnetic wave has been witnessed through the simulation of similar Tesla-type structure both in fluid dynamics and Electromagnetics. Based on the results a modified Tesla-type structure is proposed utilizing few Micro-Ring Resonators. Simulations were carried out in order to identify the most promising design. Hence for single mode waveguide propagation, a novel optical nonreciprocal system has been obtained. Nonreciprocal isolation performance was observed in all simulated Structures. An isolation ratio of 24 dB has been obtained using the proposed structure having a footprint of about 20μm×20 μm in the DWDM range (1528nm-1563nm). The results presented in this work in terms of performance and footprint show the technology is fitting for optical integration in CMOS technology.

Chapter 1

Introduction and Background

1.1 Introduction

In the modern era, an enormous amount of information is flooded through smartphones, laptops and other portable devices. Wired or wireless networks have closely connected people. Network traffic, especially mobile data traffic is growing at a so higher pace that it has not been imagined before. It has been projected that mobile data traffic will rise at a compound annual growth rate (CAGR) of 46 percent from 2017 to 2022, spanning 77.0 Exabyte's per month by 2022 as shown in Figs. 1.1 below[1]

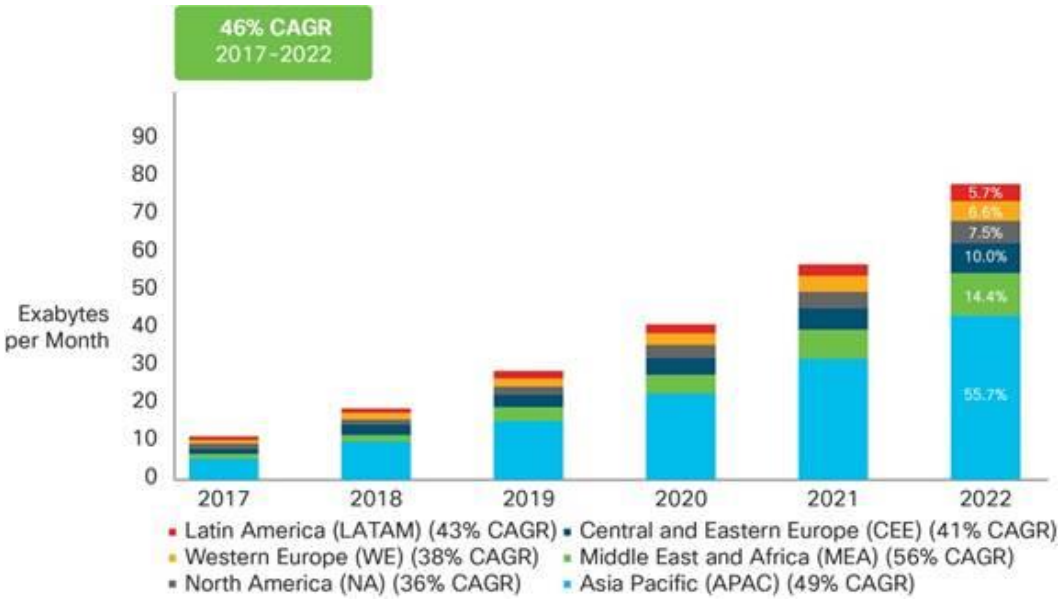

Fig. 1.1: Global mobile data traffic forecast by region

Moore's law predicts the number of transistors in a dense integrated circuit. According to Moore, the number of transistors in an IC roughly doubles in every two years. The nanometer-scale electronic device performance deteriorates sharply due to the RC time constant of the traditional metal interconnects. Therefore, the device bandwidth cannot increase at the rate Moore's law predicted.

Optics provides a platform for solving the electrically interconnect bottleneck. The bandwidth of an optical signal is significantly higher than its electronic counterparts. For example, infrared light, around 1550 nm, bandwidth is on the order of 200 THz. Besides optical signals can be transmitted by both optical waveguides and optical fibers. Both the fiber and the waveguide have significantly less loss and distortion than electronic interconnects. However, the discrete optical component packaging for building practical systems are time-consuming and expensive.

The complementary metal oxide semiconductor (CMOS) process can implement low-cost integrated devices. Silicon on Insulator (SOI) waveguides have been under active consideration for strong optical confinement contributed by the high index variance between silicon (n=3.45) and SiO2 (n=1.45) and by shriveling the dimensions of photonic devices near 1550 nm.

Wavelength division multiplexing (WDM) is a technology or technique modulating optical carrier signals of varying wavelengths of laser light, on to a single optical fiber. WDM enables bidirectional communication as well as multiplication of signal capacity. A multiplexer should not permit backscattering of light to any of the input ports. The use of optical isolators can avoid back reflection.

A crucial problem in modern photonics is optical isolation. An optical isolator permits light to pass through in one direction but hinders it in the opposite, thereby acting as the optical analogue of an electronic diode. Because that mechanism offers a preferred route for light, it must break the symmetry of Maxwell's equations known as Lorentz reciprocity [1].

Lorentz reciprocity establishes a stringent relationship between the electromagnetic fields and their sources. This phenomenon is analogous with Green's reciprocity principle for electrostatic [2, 3]. Lorentz reciprocity can inject noise into circuits and damage devices such as lasers. This injected noise may broaden the laser line width and increase the amplitude of noise.

Isolators are used to hinder unwanted feedback into the source. This feedback is capable of frequency shift, noise, mode hopping or amplitude fluctuation. Thus they play a pivotal role in blocking destabilizing feedbacks into sources to limit the generation of phase noise.[2].

Lorentz reciprocity establishes a stringent relationship between the electromagnetic fields and their sources. This phenomenon is analogous with the Green's reciprocity principle for

electrostatic[3, 4]. Lorentz reciprocity can inject noise into circuits and damage devices such as lasers. This 'injected noise ' may broaden the laser line width and increase the amplitude of noise.

1.2 Literature Review

Theoretically, the time-reversal symmetry allows the generation of new photonic states like topological states and Quantum Hall States[5]. Thus optical nonreciprocity is exceptionally challenging to implement practically. In general, breaking the time reversal symmetry is not auspicious as long as the structure is linear, time-invariant and not biased by a quantity. In practice, optical nonreciprocity is achieved by applying a static magnetic bias on the guiding path of light-matter interaction [6-9]. The commercially available optical isolators are based on Faraday rotation principle. Here constructive and destructive interference occur between two 45^{o} rotation in the backward and forward transmission, respectively. Nowadays Si based magneto-optic garnet associated isolators perform nonreciprocity in different structures like rings [10-12], Mach–Zehnder interferometer (MZI)[13-15] and periodic loading on top of normal waveguide[16]. Table 1.1 presents a summary of the conventional non-reciprocal photonic devices developed so far with their physical size and output parameters. As can be seen in the table that such devices are bulky and costly[17]. Unfortunately, these bulky components are not compatible with existing Complementary Metal-Oxide-Semiconductor(CMOS) technology[18] for integration. Additionally, the application of external magnetic inclination is also fatal to the functionality of nearby delicate components and devices. The magneto-optical garnet crystals are commonly used for obtaining non-reciprocity owing to their low optical absorption and large first order magneto-optical effect [17, 19-21]. However, the garnet crystals are difficult to grow on the widely used optical waveguide platforms like silicon [10, 17, 22, 23].

Table-1.1: SOI-based optical Isolators

Researcher	Structure	Isolation (dB)	Length of the device	Working wavelength	Year
T.Mizumoto 's group: Y.Shoji etc.[24]	MZI	>21 dB	NA	1530-1565 nm	2007
T.Mizumoto 's group: Y.Shoji etc.[25]	MZI	21 dB	4 mm	1559 nm	2008
T.Mizumoto 's group: Y.Shoji etc.[26]	MZI	18 dB	>1.5×1.5 mm^2	1322 nm	2012
T.Mizumoto 's group: Y.Shoji etc.[27]	MZI	28 dB	>1.5×1.5 mm^2	1552 nm	2013
T.Mizumoto 's group: Y.Shoji etc	MZI	>20 dB	>1.5×1.5 mm^2	1550±4 nm	2014
T.Mizumoto 's group: Y.Shoji etc.[15]	MZI	26.7 dB	>1.5×1.5 mm^2	1553 nm	2016
John E.Bowers' group: MingChun Tien etc.[28]	Ring	9 dB	1.8 mm	1550 nm	2011
John E.Bowers' group: D. Huang, P.Pintus and etc.[12]	Ring	32 dB	NA	1555nm	2016
Caroline A. Ross's Group: L. Bi etc.[10]	Ring	19.5 dB	290 μm	1550nm	2011
Caroline A. Ross's Group: X. Sun etc.[11]	Ring	13±2.2 dB	NA	1564.4nm	2015
Roel Baets' group: S.Ghosh etc.[29]	MZI	25 dB	3.46×0.46 mm	1495.2 nm	2012
Roel Baets' group: S.Ghosh etc.[30]	MZI	11 dB	1.5 mm×4 μm	1512.6nm	2012
Roel Baets' group: S.Ghosh etc.[13]	MZI	32 dB	6 mm×0.2mm	1540.5nm	2013
Mercedeh Khajavikhan [31]	Directional coupler	23 dB	NA	1555 nm	2017

The difficulties in the conventional magneto-optic technology are motivating the on-going quest for alternative tacts to break reciprocity in chip-scale devices. The additional and compelling

ways to achieve optical nonreciprocity include nonlinear structures with a spatially asymmetric refractive-index profile[32], optomechanical systems[33-36], indirect interband photonic transitions[37-42] , Parity-time symmetry breaking in micro-ring resonator structures [43-47].

Besides the conventional linear isolators, one can break the Lorentz reciprocity using Kerr or Kerr-like non-linearity[48]. The recent works have demonstrated many nonlinear optical isolators[49, 50]. The Kerr effect is an event where the refractive index of material changes because of an applied electric field, and the change in the refractive index is proportional to the square of the applied electric field[51, 52].

1.3 Isolators

Research has been conducted to develop isolators based on various structures and materials.

1.3.1Commercial Optical Isolators

The commercially available optical isolators use the Faraday rotation principle[53]. A Faraday rotor is a magneto-optic device, where light is transmitted through a transparent medium which is exposed to a magnetic field.

The direction of polarization of a linearly polarized light is continuously rotated during the route through the medium. The total rotation angle β can be defined as

$$\beta = V B L \tag{1.1}$$

Where V is the material's Verdet constant,

L is the length of the rotator and B is the magnetic flux density in the direction of propagation.

The change of polarization direction is defined only by the magnetic field direction and the sign of the Verdet constant. If some linearly polarized beam is sent through a Faraday rotator and back again after reflection at a mirror, the polarization changes of the two passes add up, rather than canceling each other.

A Faraday isolator contains three main parts, two of them are polarizers occupying a Faraday rotator in between them. When light passes through the input polarizer at forwarding bias, it becomes polarized with the vertical plane. Upon crossing through the Faraday Rotator, the plane of polarization will have been rotated 45° on axis. The output polarizer is aligned 45° relative to the input polarizer to allow light to pass unimpeded.

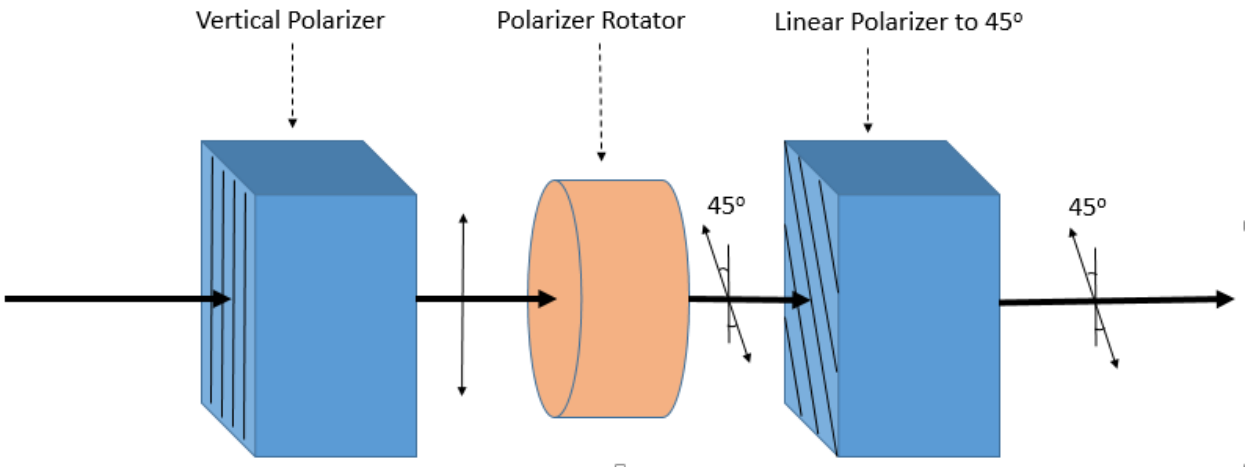

Fig. 1.2: Faraday Isolator in Forward Direction

As Fig2 shows, light traveling in the reverse direction will pass through the output polarizer and become polarized at 45°. Then the Faraday rotator will rotate the input light again by 45°. The light, being polarized in the horizontal plane will be rejected by input polarizer. Because it only allows light which is polarized in the vertical plane.

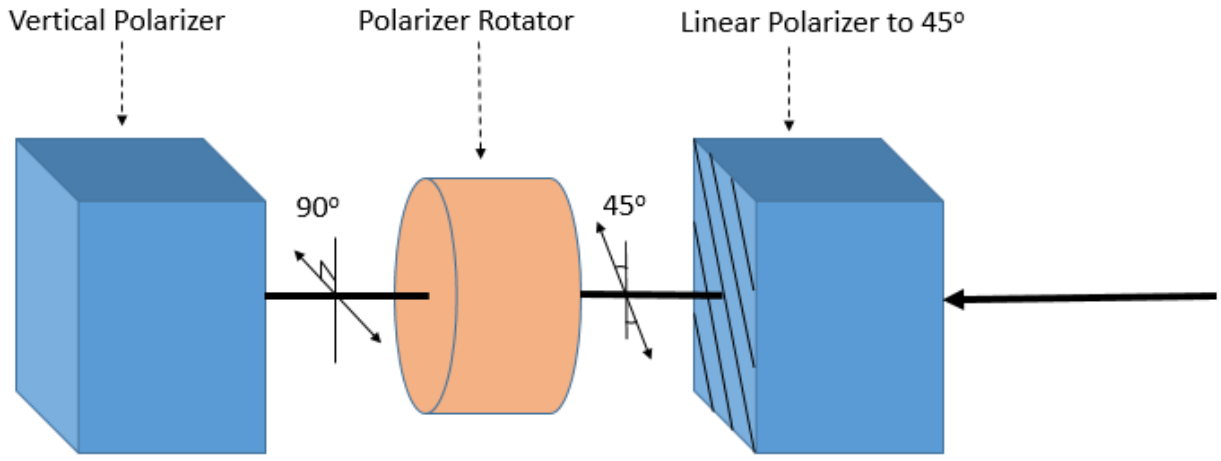

Fig 1.3: Faraday Isolator in Reverse Direction

1.3.2 Reciprocity Using Nonlinearity:

In contrast to linear isolators, Lorentz reciprocity can be broken using nonlinearity[54]. Many modern types of research have reported nonlinear isolators[49, 50]. Most of these isolators are based on third-order (or Kerr) nonlinearities, which are common in metals and don't require particular infinitesimal asymmetries in the crystal structure of optical materials to arise. The researchers have found that, though Kerr nonlinear devices can show non-reciprocal behavior to strong signals, they don't provide the same non-reciprocal response when small signals are considered in superposition with large signals.

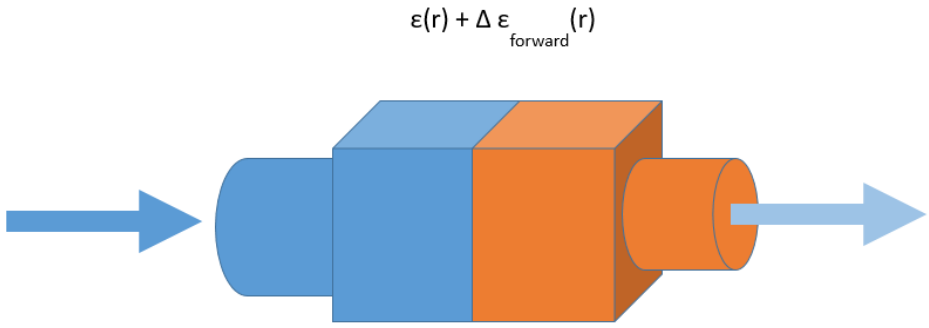

Fig 1.4: Nonlinear Isolator in Forward Direction

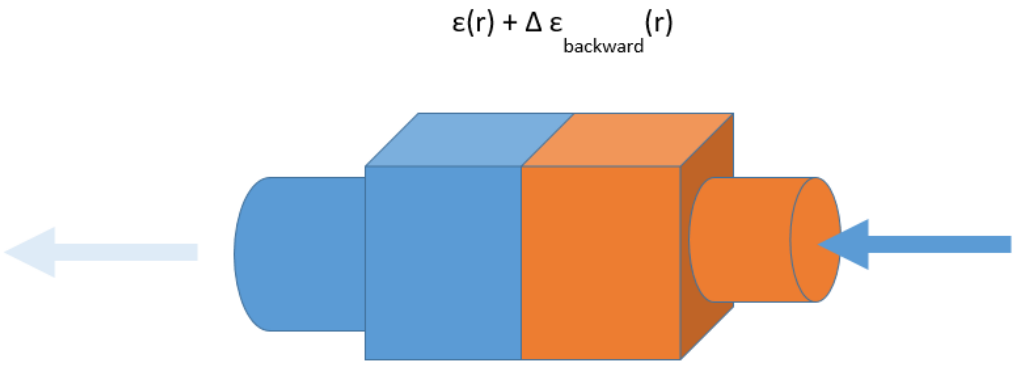

Fig 1.5: Nonlinear Isolator in Reverse Direction

Nonlinear systems based nonreciprocity is known to have some drawbacks. Similar to magneto-optical effects nonlinear responses are inadequate in the optical range. Beside that the response of the device is inherently dependent on the input intensity, forcing the strength of the isolation to be intensity-dependent and making the device prone to distortions. Hence the same nonlinearity with a combination of different waves may respond radically different from the expected device response when forward and backward waves are individually considered. However, with the recent advancements in the nanofabrication of high-quality resonators, a dramatic enhancement of nonlinear responses has been achieved on-chip.

The forward (Fig 1.3) and backward (Fig 1.4) waves encounter separate dielectric permittivity distributions due to nonlinearity. In the forward direction, the permittivity distribution is advantageous for transmission, whereas, in the backward direction, the permittivity distribution is not desirable for transmission. Here ε(r) is spatial(r) dependent permittivity distribution.

1.3.3 Optical Nonreciprocity Using Optomechanical Structures

A promising approach to break time-reversal symmetry is space-time modulation of the refractive index[55]. Space-time modulation allows two counter propagating modes to establish a form of angular momentum biasing to create nonreciprocity. It has been theoretically predicted that pronounced optical time-modulation can be realized in cavity optomechanics[34]. Researchers have found that these optomechanical interactions in ring resonators can enable a nonreciprocal response.

After the theoretical explanation of optical gradient force by parallel waveguide was given by Povinelli et al. many optomechanical structures have been proposed and demonstrated [56-60] such as nanowaveguide [61-66], microcavity[67-76] and photonic crystal cavity[77-81].

1.4 Motivation for the Research

The example of nonreciprocity or unidirectional flow is not an uncommon event. The motivation of these research came with an interesting discovery done by the renowned scientist Nikola Tesla (1856-1943). At the beginning of this research a lot about the current technology and the analogous devices in the other fields such as Diode in electronics and valve in fluid mechanics have been searched. Whatever the fields and mediums are the principle is similar, unidirectional flow. So in search of that kind of unidirectional flow it is found that Tesla had designed a fluid valve that has no movable parts inside it. The geometry of the structure is auspicious for unidirectional flow. So the structure has been analyzed and used the design to model our nonreciprocal system. The design is quite old and common in fluid mechanics but quite novel in electromagnetics. Besides that the external bias and the footprint of the device are to have scopes for improvement.

1.5 Thesis Objective

The main thesis objective is to design a novel optical nonreciprocal device for WDM application. However, more particularly, the objectives include

- Study of Reciprocity, Time reversal symmetry and breaking of Time reversal symmetry
- Study of Tesla type fluid valves and their mathematical correspondences with Electromagnetic wave theory.
- Study of S parameters to observe the non-reciprocity behavior.
- Study of Magnetic field, H_z distribution of the proposed system, which is analogues to velocity field distribution of the fluid valve.
- Comparison with existing Optical non-reciprocal system.
- Obtain the maximum possible isolation in the WDM application range(1528 nm-1563nm).

1.6 Outline of This Thesis

In the first part of this thesis in **Chapter two** the study of nonreciprocity, the Lorentz reciprocity theorem, its origin, time reversal symmetry in Electromagnetics, overview of the three fundamental types of nonreciprocal system: a) Linear Time Invariant nonreciprocal system b) Linear Time Variant nonreciprocal system c) Non-linear nonreciprocal system has been given.

Chapter Three Provides a brief Idea on the Silicon on Insulator as the designing technology and Ray model for wave propagation in SOI. A brief description about the polarization and waveguide modes, effective index of a mode and mode profiles has been done here. At the end of this chapter different types of SOI waveguide structures have been introduced along with their propagation pattern.

In **Chapter Four** the Micro Ring Resonator structures and their mathematical model has been discussed. Here a major emphasis has been given on the optical coupling. Based on that Single ring resonator with a pair of waveguides and serially coupled ring resonator model have been derived.

In **Chapter Five** the Simulation Technology and Methodology have been discussed. Here in this research CST (Computer Simulation Technology)[82] software is used as the simulation tool. The flow chart of the simulation and the solver set up will be discussed in this chapter. At the end of this chapter the basic micro ring resonator waveguides have been simulated on the SOI platform and some of their characteristics have been studied based on the literature review.

Chapter Six is the most important chapter in this thesis. The mechanical Tesla type valve has been analyzed in this chapter. A mathematical analogue between electromagnetic wave and mechanical wave has been shown here. Based on that mathematics and design a similar Tesla type

structure has been applied on the SOI technology with the help of CST simulation software. A series of experiments on that structure has been done and the pivotal observations have been noted.

Chapter Seven deals with the final proposed optical nonreciprocal structure and the field propagation and S parameters have been analyzed and the conclusion and scopes of the proposed design have been discussed here.

Chapter Eight deals with the result analysis and the future scope of the research work.

Chapter 2

Nonreciprocal Systems

2.1 Introduction to Nonreciprocity

Nonreciprocity is the deficiency of “reciprocity.” The adjective "reciprocal" comes from the Latin word "reciprocus", built on the affixes re- (backward) and pro- (forward), that merge in the phrase reque proque with the meaning of "going backward as forward". Thus, "reciprocal" basically means "going the same way backward as forward."

Usually in engineering nonreciprocity applies to systems which circumscribe media and components. Nonreciprocity considered as the property of a system where a ray of light and its reverse ray encounter different optical events – reflection, refraction, and absorption – was first explicitly described by Stokes in 1840[83] and Helmholtz in 1856[84], which led to the so-called Stokes-Helmholtz reciprocity principle. The concept was later reformulated by Kirchhoff in 1860, described as a consequence of propagation linearity by Rayleigh in 1873[85].

2.2 Time Reversal Symmetry

Time reversal means a system looks the same if the flow of time is reversed. Let the source is excited at the time, $t=0$ and the response of the system is traced until time, $t = T$ of complete transmission to sink. If the sink is now excited at a retarded time, $t = -T$ is evolving until the time, $t = 0$ of complete transmission to the source: these phenomena are called time reversal. If the system remains identical under time reversal, it is called “time-reversal symmetric".

2.3 The Lorentz Reciprocity Theorem

In classical electromagnetism, reciprocity refers to a mixture of related theorems involving the variation of time-harmonic electric current densities and the resulting electromagnetic fields in Maxwell's equations for time-invariant linear media under specified limitations. Lorentz Reciprocity theorem states that the relationship between an oscillating current and the resulting electric field is unchanged if one interchanges the points where the current is placed and where the field is measured. For the particular instance of an electrical network, it is sometimes phrased as

the statement that voltages and currents at different points in the network can be interchanged. The Green's reciprocity theorem in Electrostatic is analogous to Lorentz theorem in electromagnetics. The Green's reciprocity theorem relates the interchange of electric potential and electric charge density.

A formal etymology of the Lorentz Reciprocity Theorem[86] rises by considering a volume containing two sets of sources (current densities), J_1 and J_2, which each produce fields E_1, H_1 and E_2, H_2, respectively, as shown in Fig 2.1

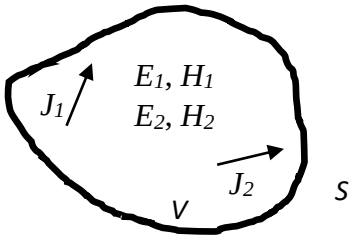

Fig. 2.1: Volume containing two electric sources

Lorentz Reciprocity can be derived by considering the quantity (divergence of the difference poynting vectors obtained by exchanging the field quantities of the sources)

$$\boldsymbol{\nabla}.(\boldsymbol{E_1} \times \boldsymbol{H_2} - \boldsymbol{E_2} \times \boldsymbol{H_1})$$

Which is expandable using a vector identity as

$$(\boldsymbol{\nabla} \times \boldsymbol{E_1}).\boldsymbol{H_2} - (\nabla \times \boldsymbol{H_2}).\boldsymbol{E_1} - (\boldsymbol{\nabla} \times \boldsymbol{E_2}).\boldsymbol{H_1} + (\boldsymbol{\nabla} \times \boldsymbol{H_1}).\boldsymbol{E_2}$$

From Maxwell's curl equations for time harmonic case,

$$\boldsymbol{\nabla} \times \boldsymbol{E_1} = -j\omega\mu\boldsymbol{H_1} \quad (2.1)$$

$$\boldsymbol{\nabla} \times \boldsymbol{H_1} = j\omega\varepsilon\boldsymbol{E_1} + \boldsymbol{J_1} \quad (2.2)$$

$$\boldsymbol{\nabla} \times \boldsymbol{E_2} = -j\omega\mu\boldsymbol{H_2} \quad (2.3)$$

$$\boldsymbol{\nabla} \times \boldsymbol{H_2} = j\omega\varepsilon\boldsymbol{E_2} + \boldsymbol{J_2} \quad (2.4)$$

Therefore,

$$\nabla.(\boldsymbol{E_1}\times\boldsymbol{H_2}-\boldsymbol{E_2}\times\boldsymbol{H_1})=-j\omega\mu\boldsymbol{H_1}.\boldsymbol{H_2}-j\omega\varepsilon\boldsymbol{E_2}.\boldsymbol{E_1}-\boldsymbol{J_2}.\boldsymbol{E_1}+j\omega\mu\boldsymbol{H_2}.\boldsymbol{H_1}+j\omega\varepsilon\boldsymbol{E_1}.\boldsymbol{E_2}+\boldsymbol{J_1}.\boldsymbol{E_2}$$

$$=\boldsymbol{J_1}.\boldsymbol{E_2}-\boldsymbol{J_2}.\boldsymbol{E_1} \tag{2.5}$$

Let us now integrate the divergence over the volume of interest:

$$\iiint\nabla.(\boldsymbol{E_1}\times\boldsymbol{H_2}-\boldsymbol{E_2}\times\boldsymbol{H_1})dv'=\iiint(\boldsymbol{J_1}.\boldsymbol{E_2}-\boldsymbol{J_2}.\boldsymbol{E_1})\,dv' \tag{2.6}$$

Applying the Divergence Theorem to the left-hand side:

$$\oiint(\boldsymbol{E_1}\times\boldsymbol{H_2}-\boldsymbol{E_2}\times\boldsymbol{H_1}).ds'=\iiint(\boldsymbol{J_1}.\boldsymbol{E_2}-\boldsymbol{J_2}.\boldsymbol{E_1})\,dv' \tag{2.7}$$

Here $\boldsymbol{E}\times\boldsymbol{H}$ points in the radial direction normal to sphere, $\hat{\boldsymbol{n}}$ and $\boldsymbol{E}$ and $\boldsymbol{H}$ are related through

$$\boldsymbol{H}=\frac{\hat{\boldsymbol{n}}\times\boldsymbol{E}}{\eta} \tag{2.8}$$

Using (2.8) the integrand on the left-hand side of (2.7) can be written as

$$(\boldsymbol{E_1}\times\boldsymbol{H_2}-\boldsymbol{E_2}\times\boldsymbol{H_1}).\hat{\boldsymbol{n}}dS=(\hat{\boldsymbol{n}}\times\boldsymbol{E_1}).\boldsymbol{H_2}-(\hat{\boldsymbol{n}}\times\boldsymbol{E_2}).\boldsymbol{H_1} \tag{2.9}$$

$$=\eta\boldsymbol{H_1}.\boldsymbol{H_2}-\eta\boldsymbol{H_2}.\boldsymbol{H_1}=0 \tag{2.10}$$

Hence

$$\iiint\boldsymbol{J_1}.\boldsymbol{E_2}\,dv'=\iiint\boldsymbol{J_2}.\boldsymbol{E_1}dv' \tag{2.11}$$

This is the form of reciprocity theorem.

2.4 Breaking Reciprocity

Afanasiev[87] has shown in detail the analytical complexities of completely characterizing source and detector in order to be able correctly to state electromagnetic reciprocity theorems. He gives conditions under which the Lorentz lemma between source and detector current densities and fields will hold. He has analyzed the assumption on the separability of time and spatial variables in charge–current densities. Afanasiev deduced that the Source having higher number of

coils at higher frequencies due to the leakage current appear between the particular turns, the current will change along the media (wire). As a result the time dependence is not now separated. This leads to the violation of the reciprocity theorem.

Landau and Liftshitz[88] had reiterated this lemma for magnetic fields

$$\iiint \boldsymbol{J_1}.\boldsymbol{H_2}\, dV = \iiint \boldsymbol{J_2}.\boldsymbol{H_1}\, dV \tag{2.12}$$

In this circumstances, only when sources are small in extent (compared with wavelengths) and current densities are given by separable functions of space position and time does Lorentz reciprocity necessarily hold. Contrarily reciprocity failure is a result of certain sorts of unusual medium response as explained below. Reciprocity of scattering of a plane incident wave, has been explicitly limited to bounded scattering media with symmetric and linear permittivity, conductivity and permeability[89]. Because they have been analyzed in terms of the electromagnetic field rather than in some scalar wave approximation. The non-reciprocal propagation that is mostly exploited in passive optical elements is linked with the gyrotropy of magneto-optic media. Another type of reciprocity breakdown is intrinsic to the wave-mixing phenomena studied in photorefractive adaptive optics. Photorefractive media are nonlocal in the sense that the gradients of fields appear in their constitutive relations and therefore, exhibits nonreciprocity.

2.5 Types of Nonreciprocal Systems

2.5.1 Linear Time-Invariant Nonreciprocal Systems

The vast majority of nonreciprocal systems are based on LTI media. The LTI media allows external bias rather than non-linearity combined with structural asymmetry to enable non-reciprocity. The non-reciprocity is achieved by breaking time reversal symmetry with the external bias. The operation can be in any arbitrary direction. It provides a high Isolation compromising the footprint of the device. Materials like Ferro-magnets, Ferrites, magnetized plasma, two-dimensional electron gases, Nano and transistor loaded materials can be used as space time modulated media for LTI nonreciprocal systems.

2.5.2 Linear Time-Variant Nonreciprocal Systems

Time Reversal symmetric breaking by time-reversal odd external bias and velocity is associated with the bias. Like LTI mediums LTV also provides a strong nonreciprocity because of linearity of the system. Moving medium (i.e., moving matter) modulation (e.g., optomechanical) and moving wave (i.e., moving perturbation) modulation produce both Doppler shift and non-reciprocity.

2.5.3 Nonlinear Nonreciprocal Systems

Time reversal symmetric is broken by means of spatial asymmetry and nonlinear self-biasing. That means nonlinearity is triggered by the signal wave itself. The operation direction is only one at a time. It has limitations to restricted excitations, intensities and isolation which represents the aspect of weak non-reciprocity.

Chapter 3

SOI Waveguides

3.1 Introduction to Waveguide

An American Engineer named Gordon Moore was asked to predict the development of silicon chip over the next decade, for a special issue of the journal Electronics in 1965. Moore observed that the number of components in these chips roughly doubled each year. Moreover, he estimated 65000 components per chip within 1975. However, as the growth in 1975 began to slow Moore revised his period for two years.

The increased speed and the capability of the processor have had an enormous impact on both our society and industry. As the components become smaller, they become faster and can conduct more electricity. Moreover, power consumption is less too. Finally, the smaller a component becomes, the production cost of each component goes down, and more of them can be packed as a chip.

Silicon on Insulator (SOI) has been under active consideration for the last 30 years as one of the faster semiconductors. The performance of Silicon components has steadily improved by shrinking their dimension. As the physical limitations of electrical interconnect the optical links has become one of the prime alternatives of electrical transmission.

3.2 Propagation Theory

The Ray model has provided a good understanding of wave propagation without the involvement of Maxwell's equation.[90] Here Snell's law describes the behavior of propagating waves in the surface between two mediums with different refractive indexes. According to that the incident wave is partly reflected and partly transmitted:

$$n_1 \sin\theta_1 = n_2 \sin\theta_2 \tag{3.1}$$

Here, n_1 and n_2 are the refractive indexes of the medium, θ_1 and θ_2 are the angles of reflection and transmission, respectively. If these angles become smaller than critical angle θ_c, then due to Total Internal Reflection there will be no transmitted wave. This angle is given by:

$$\sin \theta_c = \frac{n_2}{n_1} \tag{3.2}$$

3.3 Polarization

The fields are classified into two possible polarizations for slab wave guide: Transverse Electric (TE) and Transverse Magnetic (TM). In Transverse Electric mode the Electric field is perpendicular to the plane of incidence while In Transverse Magnetic mode the magnetic field is perpendicular to the same plane.

3.4 Waveguide Structures:

Here, the structure of SOI and all possible waveguide structures will be discussed. The configuration of a SOI wafer is shown in the figure. A silicon dioxide layer is grown under the surface of silicon substrate. The top silicon substrate then work as the guiding layer. The buried oxide layer prevents the field associated with optical modes from penetrating the silicon substrate below. Therefore, the oxide layer must be thicker than the evanescent fields associated with the optical modes.

The refractive indices of both air ($n = 1$) and silicon dioxide ($n \sim 1.5$) are so different from that of silicon ($n \sim 3.5$) that the waveguide is transformed from asymmetrical to symmetrical one.

Optical waveguides generally can be of five types.

a. Slab type waveguide
b. Rib type wave guide
c. Ridge type waveguide

Rectangular waveguide

d. Cylindrical waveguide
e. Strip Nano Waveguide

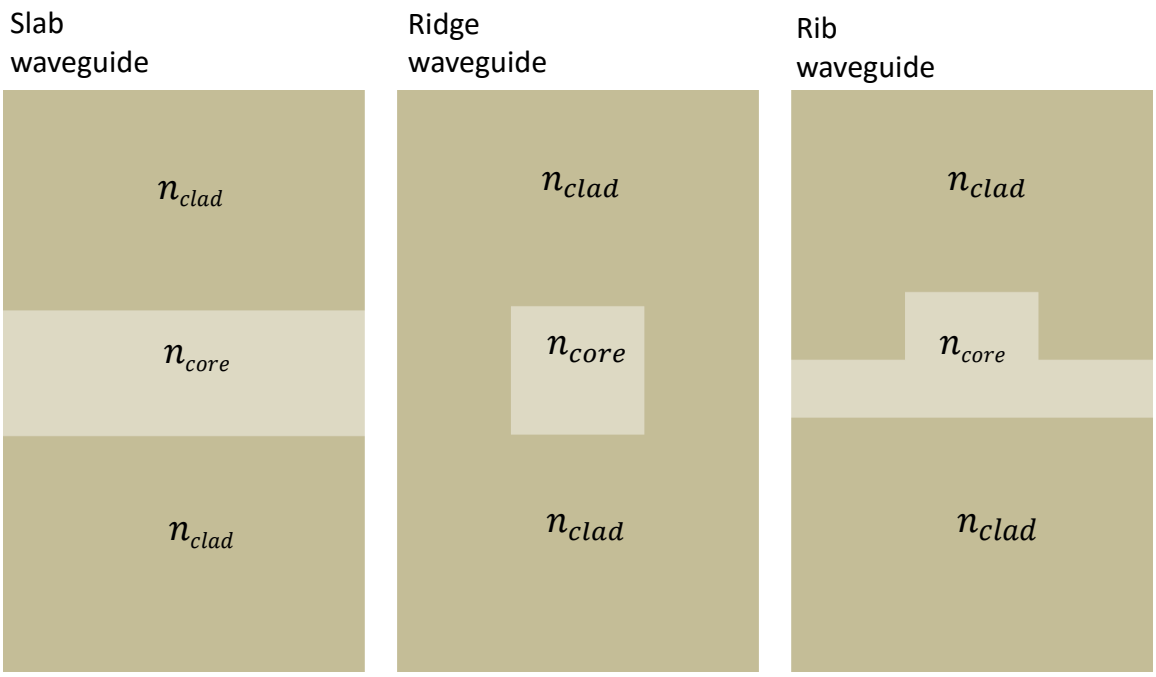

Fig. 3.1: Rectangular waveguide

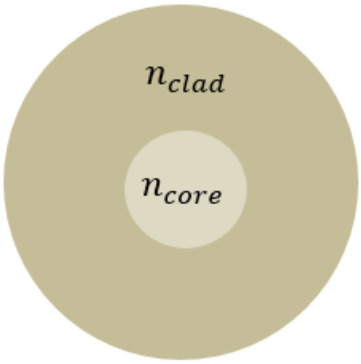

Fig. 3.2: Cylindrical waveguide

3.5 Waveguide Modes

A mode is a time harmonic solution of Maxwell's equations. Its spatial field distribution doesn't change with propagation. Waveguide modes are obtained by the cross sectional refractive index profile of the waveguide. Light only propagates in a set of allowed discrete angles. The following Equation represents the TE mode for general asymmetric waveguide[91].

$$k_0 n_1 h \cos\theta_1 - m\pi = tan^{-1}\frac{\sqrt{sin^2\theta_1 - \left(\frac{n_2}{n_1}\right)^2}}{cos\theta_1} + tan^{-1}\frac{\sqrt{sin^2\theta_1 - \left(\frac{n_3}{n_1}\right)^2}}{cos\theta_1} \qquad (3.3)$$

Here $k_0 = \frac{2\pi}{\lambda_0}$ is the propagation constant in free space and *h* is the height of the core layer. For every interface the critical angle is different; so for ensuring Total Internal Reflection the largest critical angle is the one which gives the solution.

Equation 3.3 can derive the monomode condition. The mode of propagation allows every angle to place a specific field. The mode number is indicated with index *m*. The monomode has *m=0.* In multimode waveguide the total transmitted power needs to be shared by all the modes. In addition, they suffer from Intermodal dispersion, which is caused by different velocities with which every mode travels in the waveguide. Hence throughout this research work single mode waveguide has confined our focus only.

3.5.1 Effective Index of a Mode

The propagation constant in the z direction k_z can be described by the following equation

$$k_z = n_1 k_0 sin\theta_1 \tag{3.4}$$

Here $N = n_1 sin\theta_1$ can be defined as the effective index of the mode. It denotes mode propagation in the Z direction without any reflection in the interfaces.

3.5.2 Mode Profiles in SOI Planner Waveguide

The mode profiles inside a waveguide can be derived by solving wave eq1uations subjected to appropriate boundary conditions. Away from the boundary the time harmonic electromagnetic fields in a source free region must satisfy the vector Helmholtz equation

$$(\nabla^2 + \omega^2 \mu\epsilon)\mathbf{E} = 0 \tag{3.5}$$

$$(\nabla^2 + \omega^2 \mu\epsilon)\,\mathbf{H} = 0 \tag{3.6}$$

Both the electric and magnetic field have the components in the X, Y and Z direction, so the equation for Ex would be

$$(\nabla^2 + \omega^2 \mu\epsilon)\boldsymbol{E_x} = 0 \tag{3.7}$$

$$\frac{\partial^2 \boldsymbol{E_x}}{\partial x^2} + \frac{\partial^2 \boldsymbol{E_x}}{\partial y^2} + \frac{\partial^2 \boldsymbol{E_x}}{\partial z^2} + (\omega^2 \mu\epsilon)\boldsymbol{E_x} = 0 \tag{3.8}$$

Using variable separation method (product solution of partial differential equation) let us assume

$$E_x = X(x)Y(y)Z(z) \tag{3.9}$$

Putting Ex in scalar Helmholtz equation to find

$$X = A_x e^{\pm jk_x x} \tag{3.10}$$

$$Y = A_y e^{\pm jk_y y} \tag{3.11}$$

$$Z = A_z e^{\pm jk_z z} \tag{3.12}$$

$$k_x^2 + k_y^2 + k_z^2 = k^2 = \omega^2 \mu \epsilon \tag{3.13}$$

Here, k_x, k_y, k_z and k are wave vectors.

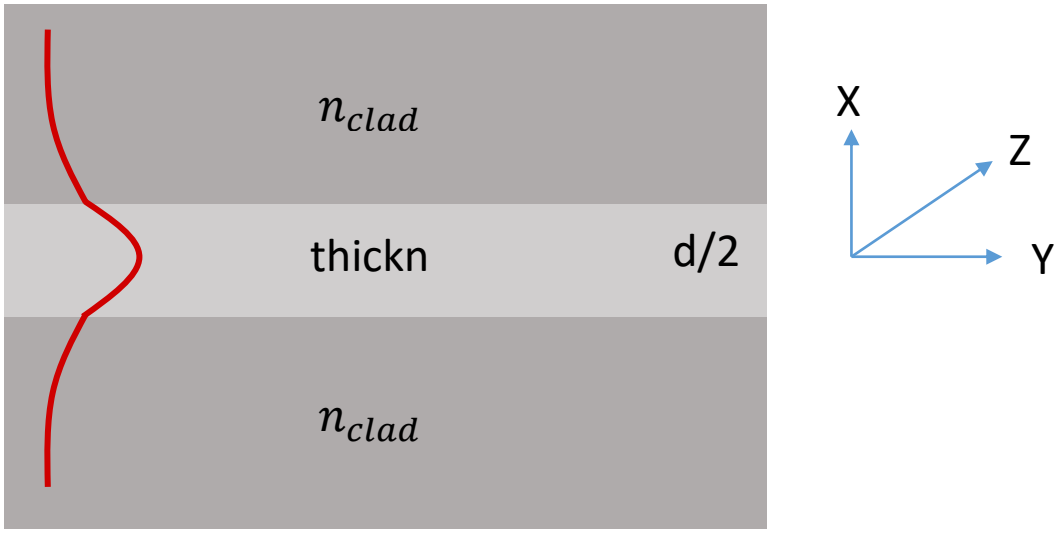

Fig. 3.3: TE_0 mode in a slab type waveguide

The same can be done for other Electric and magnetic field components.

For TE mode the E-field only has a component in the y-direction. Assuming for a wave guided along the z-direction also recognize that the structure is y-invariant

Therefore the Helmholtz equation can be simplified:

$$\frac{\partial^2 \boldsymbol{E_y}}{\partial x^2} + \cancel{\frac{\partial^2 \boldsymbol{E_y}}{\partial y^2}} + \frac{\partial^2 \boldsymbol{E_y}}{\partial z^2} + (\omega^2 \mu \epsilon)\boldsymbol{E_y} = 0$$

$$\frac{\partial^2 \boldsymbol{E_y}}{\partial x^2} + \frac{\partial^2 \boldsymbol{E_y}}{\partial z^2} + (\omega^2 \mu \epsilon)\boldsymbol{E_y} = 0 \tag{3.14}$$

The general solution will take the form of

$$\boldsymbol{E_y} = e^{jk_z z} \begin{cases} A_{y0} e^{\pm jk_{x1} x} & |x| \geq d/2 \\ A_{y1} e^{\pm jk_{x2} x} & |x| \leq d/2 \end{cases}$$

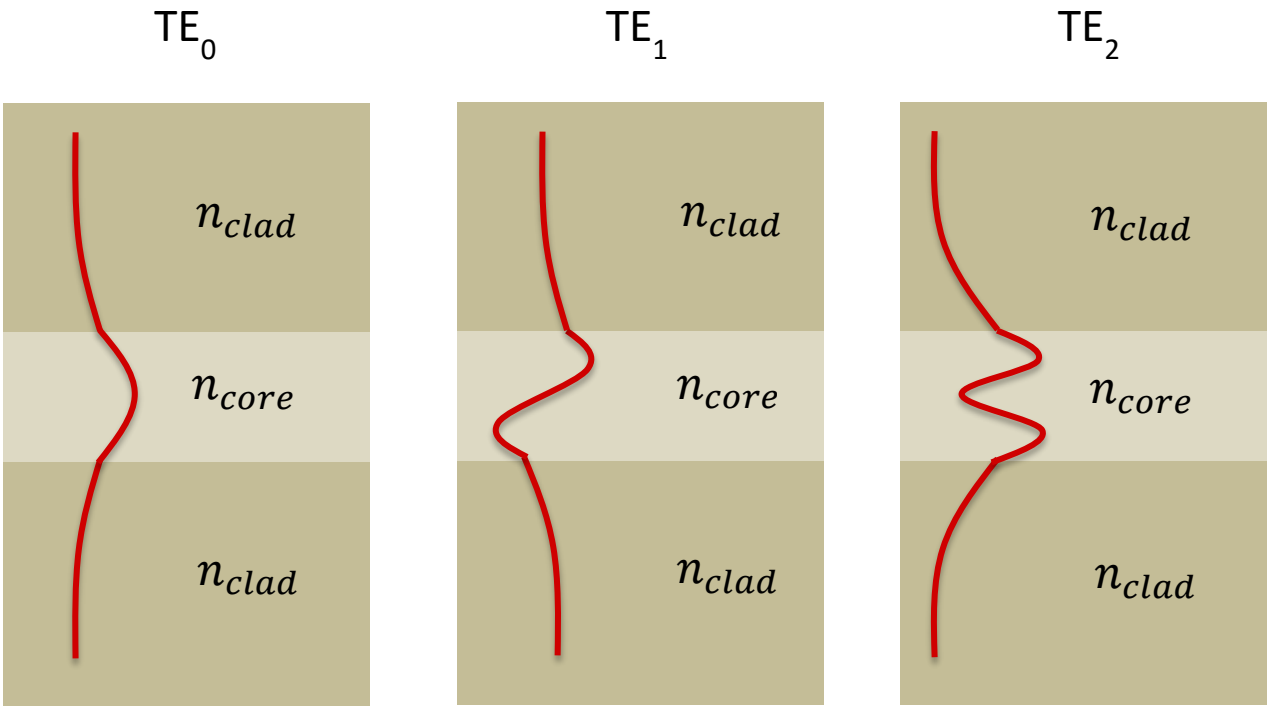

Fig. 3.4: TE modes in a slab type waveguide

3.6 Strip Nano Waveguides:

In order to get higher light confinement, the strip waveguide technology has been used. In order to use SOI waveguides for optical communications, both polarization insensitivity and single mode propagation have to be simultaneously fulfilled. The strip guided path of silicon has a structure of 0.445μm×0.22μm to facilitate the single mode only. As the input field is launched in the cladding and then couples to the core importance should be given for calculation of the Silicon Di oxide layer's width and thickness. Here the thickness of the Silicon Di oxide layer is considered 1μm. And width 2 μm for straight waveguide. For any other structures the width may be adjusted but the thickness is fixed. The detail structure dimensions of the strip waveguide has been given by the CST Support Ticket.

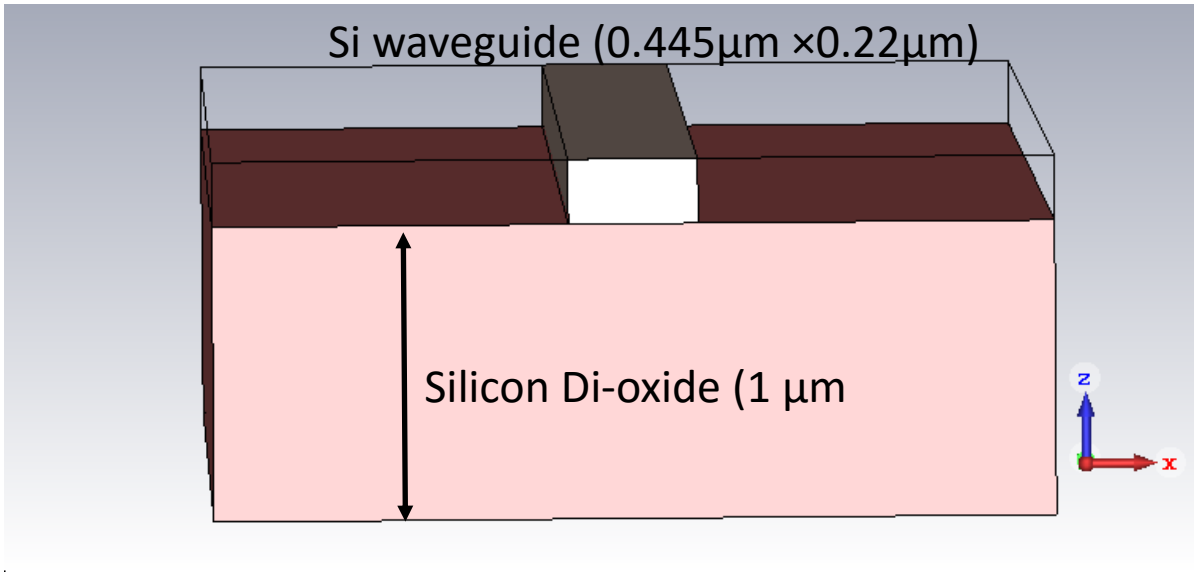

Fig 3.5: Strip Nano waveguide

Chapter 4

Optical Ring Resonator Theory and Modeling

4.1 Introduction to Optical Ring Resonator

Passive silicon waveguide structures have been recognized for the unprecedented reduction in the footprint of waveguides. Among these structures the wavelength selective devices are dominant. Ring resonators are the classic exemplar of these. Because silicon enables ring resonators of unprecedented small size. The generic structure of a ring resonator consists of an optical waveguide which is looped back on itself along with one or many straight waveguides. Resonance happens when the optical path length of the resonator is precisely a whole number of wavelengths. Therefore, ring resonators support multiple resonances.

4.2 Single Ring Resonators

4.2.1 Ring Structure with One Straight Waveguide

The basic configuration of a ring resonator consists of unidirectional coupling between a ring resonator with radius r and a waveguide[92]. The mathematical modelling has its obtained form and can be summarized below[93].

Assuming that the coupling is lossless, a single unidirectional mode of the resonator is excited and single polarization is considered the interaction can be described by the matrix relation:

$$\begin{pmatrix} E_{t1} \\ E_{t2} \end{pmatrix} = \begin{pmatrix} t & k \\ -k^* & t^* \end{pmatrix} \begin{pmatrix} E_{i1} \\ E_{i2} \end{pmatrix} \tag{4.1}$$

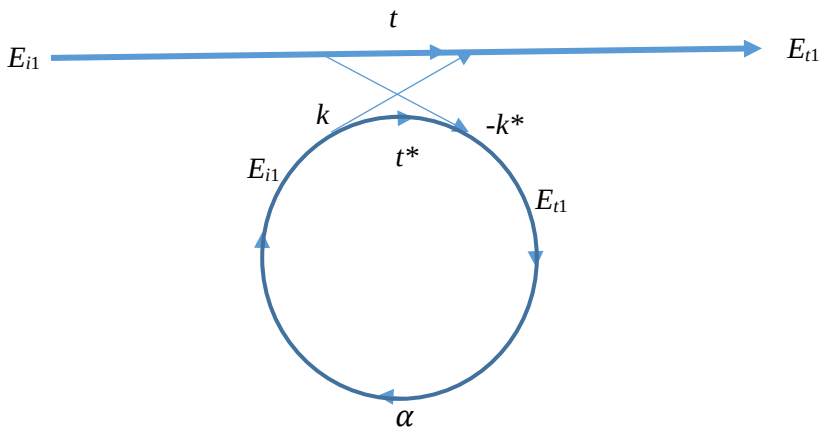

Fig.4.1: Single ring resonator with one straight waveguide

Here ***t*** is the transmission coefficient through the coupler and ***k*** is the taper-sphere mode coupling amplitude also known as the coupling coefficient. The * denotes the conjugated complex value of ***t*** and ***k***.

The network under consideration is reciprocal. Therefore,

$$|k^2| + |t^2| = 1 \tag{4.2}$$

For simplification let us choose $E_{i1} = 1$. Then the round trip in the ring is given by [93]

$$E_{i2} = \alpha . e^{j\theta} E_{t2} \tag{4.3}$$

Here α is the loss coefficient of the ring; for no loss condition, $= 1$,$\theta = \omega L/c$, L being the circumference of the ring, c the phase velocity of the ring mode ($c = c_0/n_{eff}$) and the fixed angular frequency $\omega = kc_0$, c_0 refers to the speed of light in vacuum. k can be defined using wavelength, λ; $k = 2\pi/\lambda$.

The propagation constant β can be defined as

$$\beta = k . n_{eff} = \frac{2\pi . n_{eff}}{\lambda} \tag{4.4}$$

This leads to

$$\theta = \frac{\omega L}{c} = \frac{k c_0 L}{c} = k.n_{eff}.2\pi r = \frac{2\pi.n_{eff}.2\pi r}{\lambda} = 4\pi^2.n_{eff}.\frac{r}{\lambda} \tag{4.5}$$

From equation (4.1) and (4.3) we obtain

$$E_{t1} = \frac{-\alpha + t.e^{-\mathrm{j}\theta}}{-\alpha t^* + e^{-\mathrm{j}\theta}} \tag{4.6}$$

$$E_{i1} = \frac{-\alpha k^*}{-\alpha t^* + e^{-\mathrm{j}\theta}} \tag{4.7}$$

$$E_{t2} = \frac{-k^*}{1 - \alpha t^* e^{\mathrm{j}\theta}} \tag{4.8}$$

The complex mode amplitudes *E* are normalized, so that their squared magnitude corresponds to the modal power. This leads to the transmission power P_{t1} in the output waveguide [93],

$$P_{t1} = |E_{t1}|^2 = \frac{\alpha^2 + |t|^2 - 2\alpha|t|\cos(\theta + \varphi_t)}{1 + \alpha^2|t|^2 - 2\alpha|t|\cos(\theta + \varphi_t)} \tag{4.9}$$

Where $t = |t|e^{\mathrm{j}\varphi_t}$, $|t|$ representing the coupling losses and φ_t the phase of the coupler.

$$P_{i2} = |E_{i2}|^2 = \frac{\alpha^2(1 - |t|^2)}{1 + \alpha^2|t|^2 - 2\alpha|t|\cos(\theta + \varphi_t)} \tag{4.10}$$

At resonance, $(\theta + \varphi_t) = 2\pi N$, where N is an integer number, so from (4.9),

$$P_{t1} = |E_{t1}|^2 = \frac{(\alpha - |t|)^2}{(1 - \alpha|t|)^2} \tag{4.11}$$

$$P_{i2} = |E_{i2}|^2 = \frac{\alpha^2(1 - |t|^2)}{(1 - \alpha|t|)^2} \tag{4.12}$$

An interesting scenario will occur when $\alpha = |t|$ in (4.11), the internal losses are equal to the coupling losses. The transmitted power becomes 0. This phenomenon has been mentioned in literature as critical coupling, which is due to destructive interference.

4.2.2 Ring Structure with Two Straight waveguides

Here the basic ring resonator add-drop configuration will be discussed. This structure consists of an input waveguide and an output waveguide along with a ring resonator. The four ports are referred to in the following as input port, throughput port, drop port and add port.

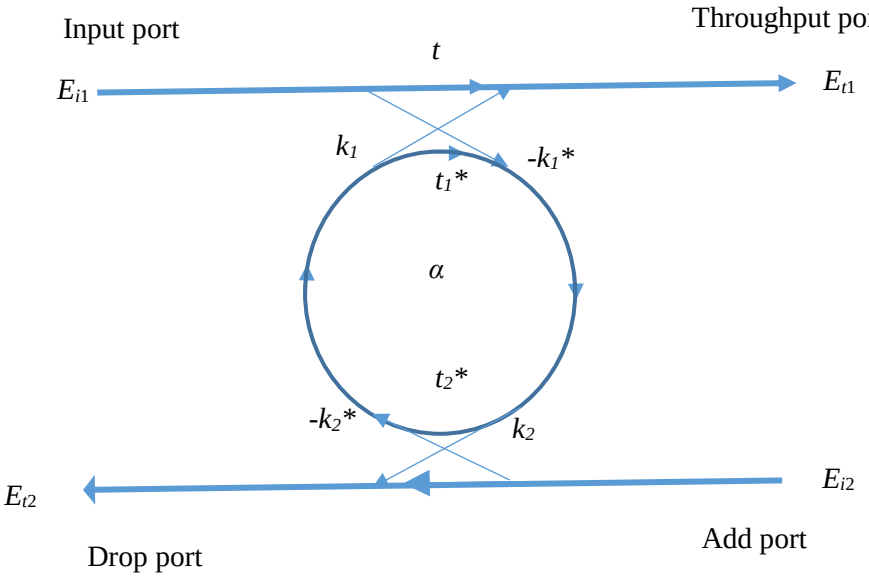

Fig. 4.2: Single ring resonator with two straight waveguide

After updating the ring resonator simulation model according to fig: 2 the throughput mode amplitude in the first waveguide is given by [93],

$$E_{t1} = t_1 + \frac{-k_1 k_1^* t_2^* \alpha_{1/2}^2 e^{j\theta(|t|^2+|k_1|^2)}}{1 - t_1^* t_2^* \alpha_{1/2}^2 e^{j\theta}} = \frac{t_1 - t_2^* \alpha_{1/2}^2 e^{j\theta}}{1 - t_1^* t_2^* \alpha_{1/2}^2 e^{j\theta}} = \frac{t_1 - t_2^* \alpha e^{j\theta}}{1 - t_1^* t_2^* \alpha e^{j\theta}} \quad (4.13)$$

In this calculation, $\alpha_{1/2}$ and $\theta_{1/2}$ are half round trip loss and phase, respectively. Thus $\alpha = \alpha_{1/2}^2$ and $\theta = 2\theta_{1/2}$

The mode amplitude in the ring has to pass the second coupler. The dropped mode amplitude in the second waveguide is given by E_{t2}.

$$E_{t2} = \frac{-k_1^* k_2 \alpha_{1/2} e^{j\theta_{1/2}}}{1 - t_1^* t_2^* \alpha e^{j\theta}} \quad (4.14)$$

At resonance the output power from the drop port is given by,

$$P_{t2-Resonance} = |E_{t2-Resonance}|^2 = \frac{(1 - |t_1|^2).(1 - |t_1|^2).\alpha}{(1 - \alpha|t_1 t_2|)^2} \quad (4.15)$$

At resonance the throughput mode amplitude E_{t1} will be zero for identical symmetrical couplers $t_1 = t_2$ if $\alpha = 1$. That indicates that the wavelength on resonance is fully extracted by the resonator.

In order to substantiate the theatrical modeling the system has been simulated to observe the electromagnetic wave flow pattern a simulation has been done in CST on SOI platform. Here, for single mode propagation it is depicted that the flow direction is similar to the direction that has been derived in theory. The Straight waveguides simulated here having dimension 0.445μm×0.22μm and the radius of the ring is 1.5 μm.

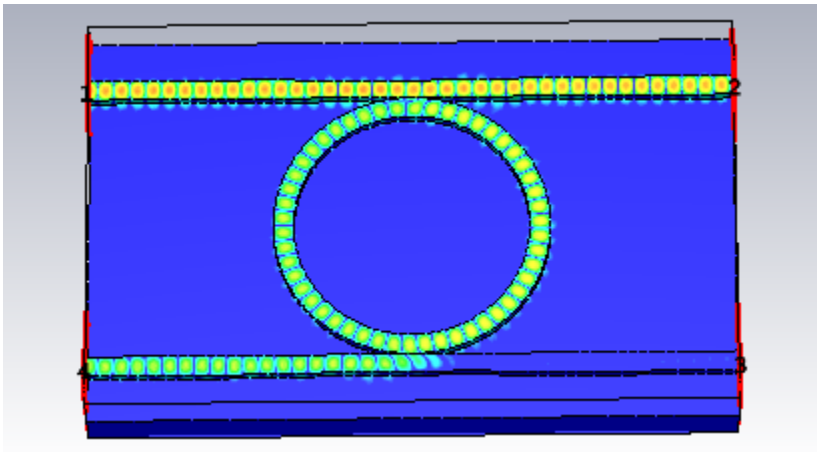

Fig. 4.3: Magnetic field, Hz distribution in Single ring resonator with two straight waveguide

4.3 Ring Resonators Figure of Merits

The performance of a ring resonator can be described by the same figures of merit which are also generally used to describe optical filters. The distance between resonance peaks is one of the important figure. The literature called that free spectral range (FSR).

From (4.4) a simple approximation of FSR by neglecting the wavelength dependence of the effective index can be obtained [93]

$$\frac{\partial \beta}{\partial \lambda} = -\frac{\beta}{\lambda} + k\frac{\partial n_{eff}}{\partial \lambda} \approx \frac{\lambda^2}{n_{eff}L} \tag{4.16}$$

This leads to FSR, which is the difference between the vacuum wavelengths corresponding to two resonant conditions.

$$FSR = \Delta\lambda = -\frac{2\pi}{L}\left(\frac{\partial \beta}{\partial \lambda}\right)^{-1} \approx \frac{\lambda^2}{n_{eff}L} \tag{4.17}$$

If the wavelength dependence of the effective index cannot be neglected, it can be incorporated in the following way to obtain a modified version of (4.16)

$$\frac{\partial \beta}{\partial \lambda} = -\frac{k}{\lambda} n_g \tag{4.18}$$

Here n_g is the group index, which is defined as:

$$n_g = n_{eff} - \lambda \frac{\partial n_{eff}}{\partial \lambda} \tag{4.19}$$

The group refractive index can be used instead of the effective index whenever appropriate avoiding the approximation and obtain more accurate values. The modified FSR is then

$$FSR = \Delta\lambda = \frac{\lambda^2}{n_g L} \tag{4.20}$$

Another important figure is the resonance width which is defined as the full width at half maximum or 3 dB bandwidth 2δλ of the resonance line shape. Using the expressions for the drop port (4.14) and (4.15)

$$\left| \frac{-k_1^* k_2 \alpha_{1/2} e^{j\theta_{1/2}}}{1 - t_1^* t_2^* \alpha e^{j\theta}} \right|^2 = \frac{1}{2} \frac{|k_1|^2 |k_2|^2 \alpha}{(1 - \alpha |t_1 t_2|)^2} \tag{4.21}$$

Assuming that the coupling coefficients are real, lossless, and without a phase term, (4.21) can be written as [93]

$$\frac{\left(k_1 k_2 \alpha_{1/2}\right)^2}{1 - 2t_1 t_2 \alpha \cos(\theta) + (t_1 t_2 \alpha)^2} = \frac{1}{2} \frac{{k_1}^2 {k_2}^2 \alpha}{(1 - \alpha t_1 t_2)^2} \tag{4.22}$$

(4.22) can be further written as

$$2(1 - \alpha t_1 t_2)^2 = 1 - 2t_1 t_2 \alpha \cos(\theta) + (t_1 t_2 \alpha)^2 \tag{4.23}$$

For small θ, using the real part of the series expansion of the Euler formula

$$\cos(\theta) = 1 - \frac{(\theta)^2}{2} \tag{4.24}$$

Therefore,

$$\theta^2 = \frac{(1-\alpha t_1 t_2)^2}{t_1 t_2 \alpha} \tag{4.25}$$

This can be further simplified if the loss in the ring is negligible and coupling is symmetric *($t = t_1 = t_2$)*

$$\theta = \sqrt{\frac{(1-t^2)^2}{t^2}} = \frac{(1-t^2)}{t} \tag{4.26}$$

Using (4.5) and (4.17) to translate into the wavelength domain

$$2\delta\lambda = \frac{\lambda^2}{\pi n_{eff} L} \frac{(1-t^2)}{t} \tag{4.27}$$

The expression which is commonly used can be obtained by assuming weak coupling and $\lambda >> \delta\lambda$

$$FWHM = 2\delta\lambda = \frac{k^2\lambda^2}{\pi n_{eff} L} \tag{4.28}$$

The rest two figure of merits are finesse *F* and quality factor *Q*. *F* is defined as the ratio of the FSR and the width of a resonance for a specific wavelength (FWHM):

$$F = \frac{FSR}{FWHM} = \frac{\Delta\lambda}{2\delta\lambda} = \pi \frac{t}{1-t^2} \tag{4.29}$$

A parameter which is closely related to the finesse is the quality factor, *Q* of a resonator, which is the measure of the sharpness of the resonance. It is defined as the ratio of the operation wavelength and the resonance width

$$Q = \frac{\lambda}{2\delta\lambda} = \pi \frac{n_{eff} L}{\lambda} \frac{t}{1-t^2} = \frac{n_{eff} L}{\lambda} F \tag{4.30}$$

The quality factor can also be regarded as the stored energy divided by power lost per optical cycle.

4.4 Serially Coupled Double Ring Resonator

In this thesis serially coupled double ring resonator has been used to design optical nonreciprocal system.

The schematic of a serially coupled double ring resonator is depicted in Fig. 4.4.

From this model and using the same procedure as in sect. 4.1.1 [93] the fields depicted in fig. can be calculated as follows:

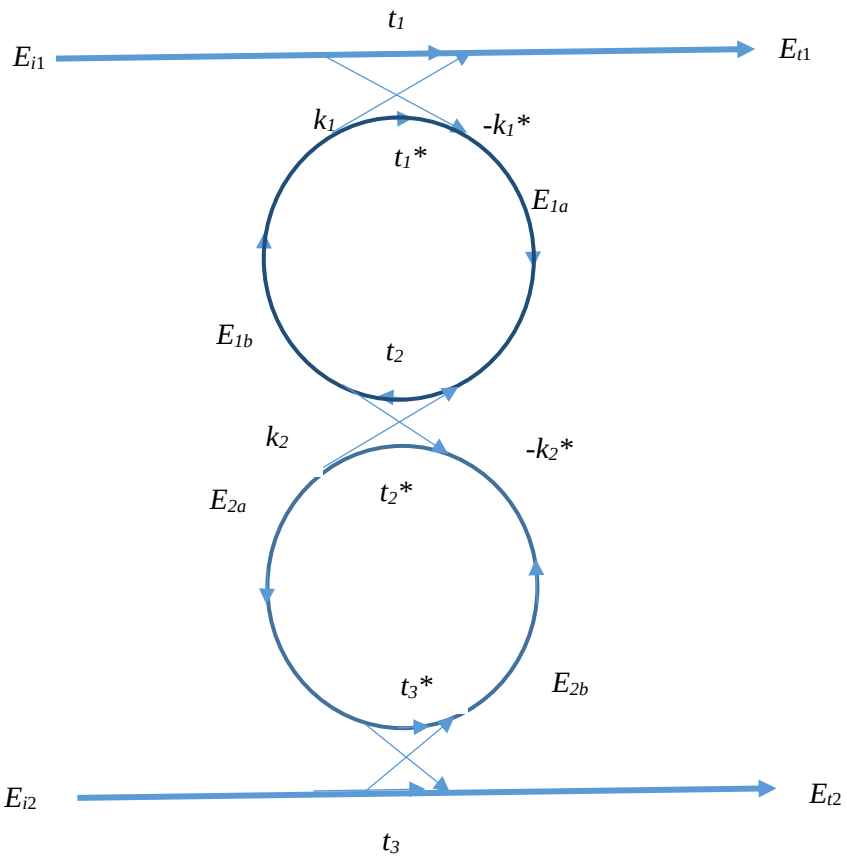

Fig. 4.4: Double ring resonator with two straight waveguide

$$E_{1a} = -k_1^* E_{i1} + t_1^* \alpha_1 e^{j\frac{\theta_1}{2}} E_{1b} \tag{4.31}$$

$$E_{1b} = t_2^* \alpha_1 e^{j\frac{\theta_1}{2}} E_{1a} + k_2^* \alpha_2 e^{j\frac{\theta_1}{2}} E_{2b} \tag{4.32}$$

$$E_{2a} = k_2\alpha_1 e^{j\frac{\theta_2}{2}}E_{1a} + t_2\alpha_2 e^{j\frac{\theta_2}{2}}E_{2b} \quad (4.33)$$

$$E_{2b} = -k_3^* E_{i2} + t_3^*\alpha_2 e^{j\frac{\theta_2}{2}}E_{2a} \quad (4.34)$$

$$E_{t1} = t_1 E_{i1} + k_1\alpha_1 e^{j\frac{\theta_1}{2}}E_{1b} \quad (4.35)$$

$$E_{t2} = t_3 E_{i2} + k_3\alpha_2 e^{j\frac{\theta_2}{2}}E_{2a} \quad (4.36)$$

Here $\alpha_{1,2} = \alpha_{R1_{1/2},R2_{1/2}}$ represent the half round trip loss coefficients of ring resonator one and two respectively.

The serially coupled double ring resonator has been simulated to verify the flow direction that has been derived in this chapter. Again the matching of flow pattern has been obtained and shown in Fig. 4.5. The Straight waveguides simulated here having dimension 0.445μm×0.22μm and the radius of the ring is 1.5 μm.

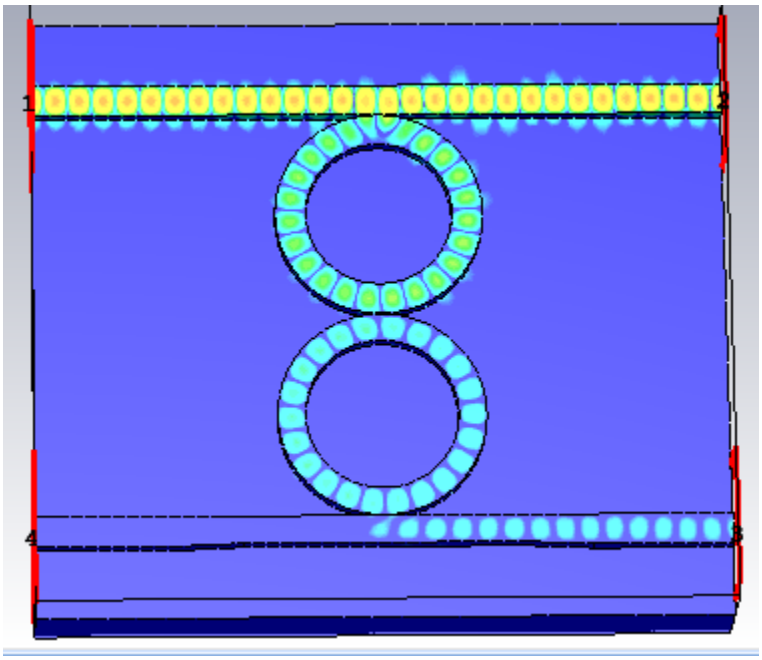

Fig. 4.5: Magnetic field, Hz distribution of Double ring resonator with two straight waveguide

Chapter 5

SOI Waveguide Simulation

5.1 Introduction to CST

Analytical calculations, using Coupled Mode Theory, are not sufficient to provide the required accuracy for Optical Ring Resonator design. They do not account for multiple reflections very easily, nor scattering and delay. Therefore, professional photonic CAD tools are needed for modeling and validation. In this thesis, CST Microwave Studio (MWS) has been used as a simulation engine to simulate light propagation.

In this chapter the simulation process will be described in brief along with the flow chart of the process of simulating Silicon on Insulator based waveguide in CST.

5.2 CST Work Flow

CST Micro Wave Studio (MWS) is a specialist tool for EM simulation high frequency components. CST MWS enables the fast and accurate analysis of high frequency (HF) devices such as antennas, filters, couplers, planar and multi-layer structures and SI and EMC effects. Here in this thesis MWS has been rigorously used for simulating SOI based waveguides. MWS has a vast domain for simulation. For SOI waveguide simulation here the following domain and work flow have been followed.

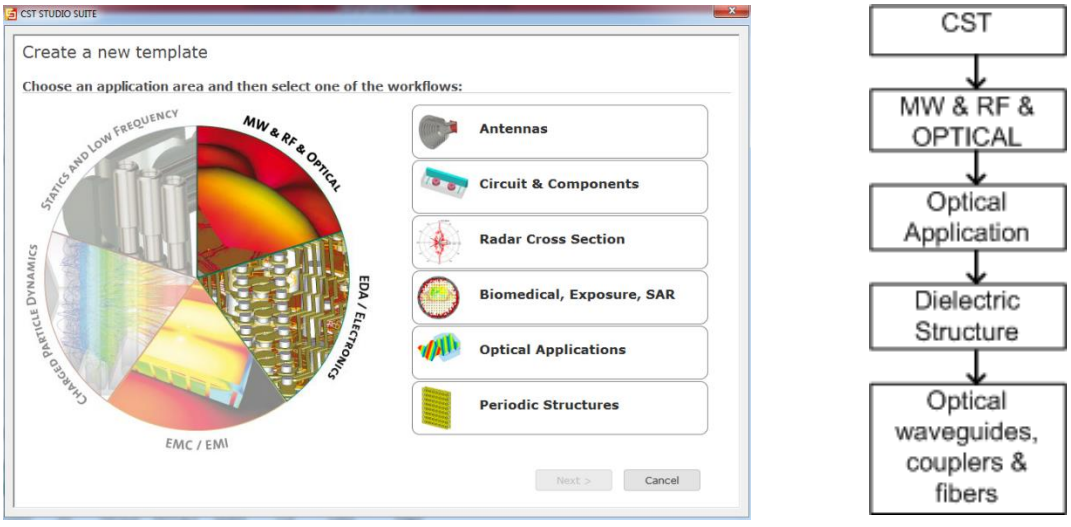

Fig. 5.1: CST simulation workflow for this thesis

The work flow to simulate any SOI device in MWS has described below (**Fig:5.2**)

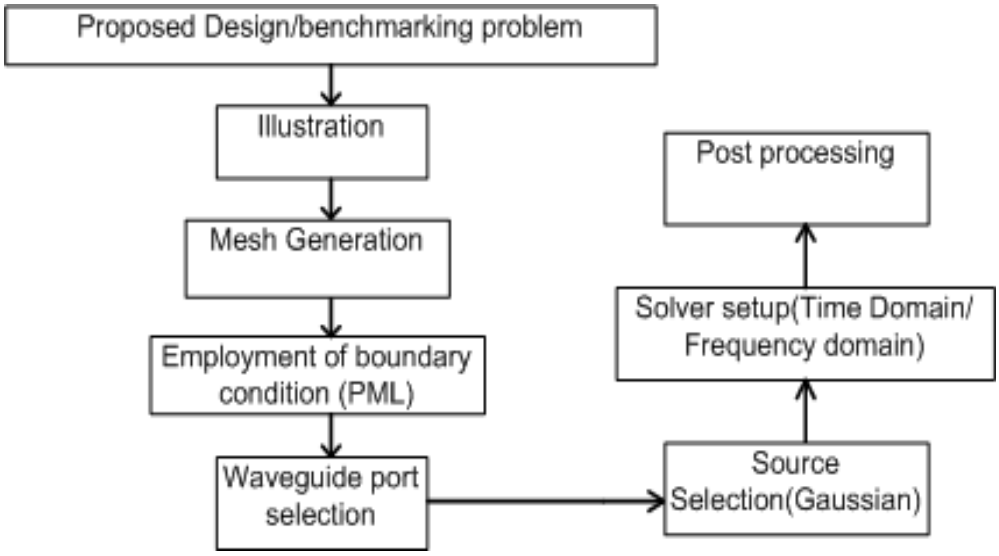

Fig. 5.2: MWS simulation workflow for this thesis

The work flow has been described here.

5.2.1 Illustration of Proposed Design

For single mode propagation our structure has some limitations in some measurements. Like to facilitate single mode propagation in SOI the width of the device is restricted to 0.445 μm and the height is 0.22 μm.

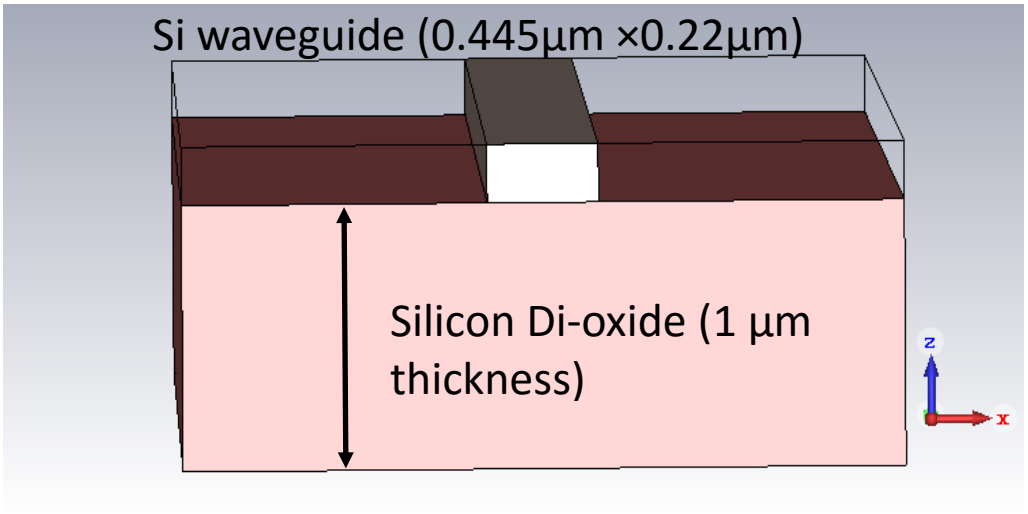

Fig. 5.3: SOI based single mode straight waveguide

5.2.2 Mesh Generation

The CST can do two types of meshing for Frequency domain calculations.

- Hexahedral
- Tetrahedral

Throughout the modelling of this research the tetrahedral meshing has been used.

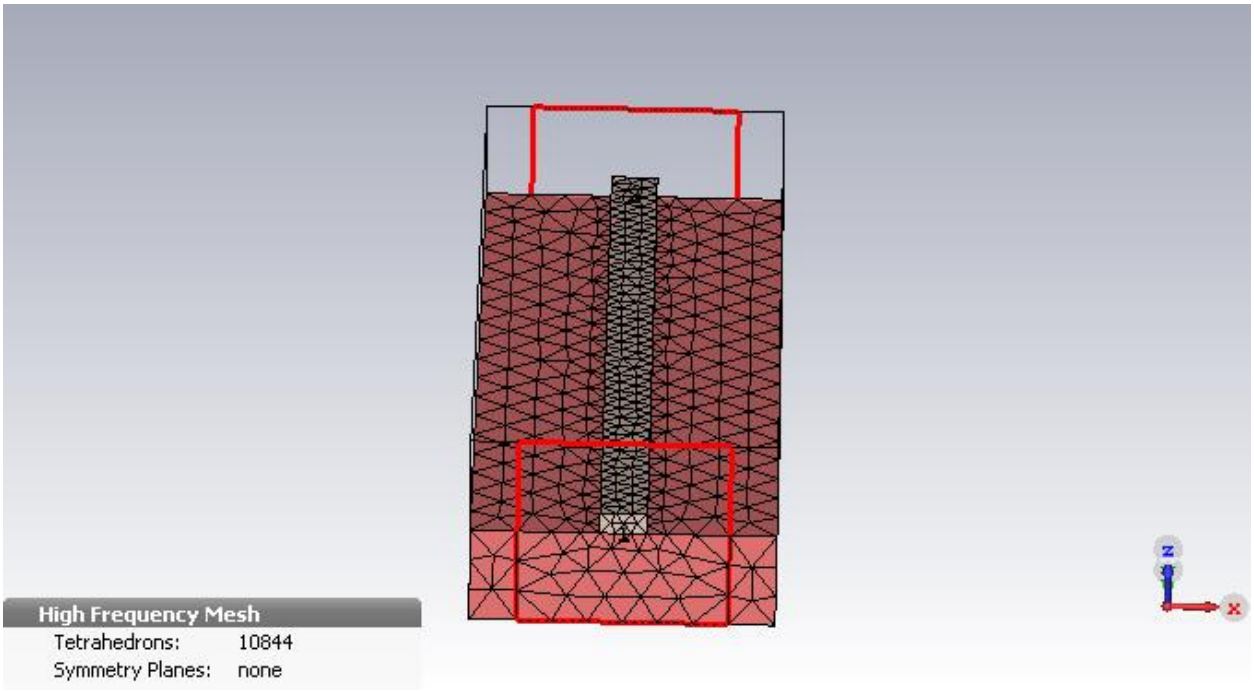

Fig. 5.4: Tetrahedral meshing of SOI waveguide

5.2.3 Employment of Boundary Condition

Throughout in this thesis PML (Perfectly Matched Layer) has been used as the boundary condition. In CST it is known as OPEN BOUNDARY.

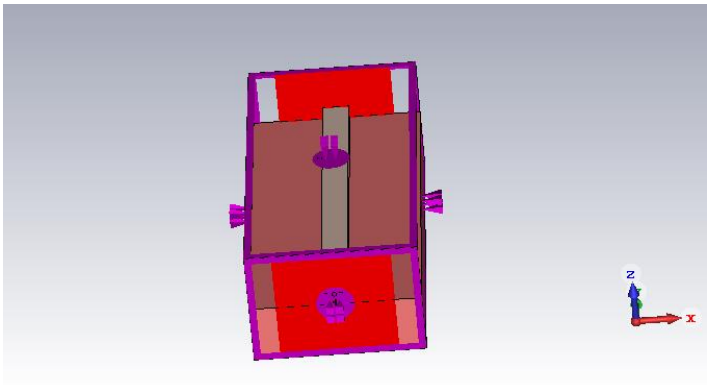

Fig. 5.5: Open Boundary condition

5.2.4 Waveguide Port Selection

A face needs to be selected to act a waveguide. This is done using the PICK FACE option. Then port extension coefficient needs to be provided by the user. Here for this thesis the ports have been extended from the center of the face to 1 μm in rectangular distance.

5.2.5 Source Selection and Solver Set up:

In CST both the Time Domain and Frequency Domain solvers are present. Here in this thesis frequency domain solver will be used, because it has faster performance than the other one. The Frequency Domain solver uses FEM (Finite Element Method). The Gaussian wave will be our source as it contains all the frequency components.

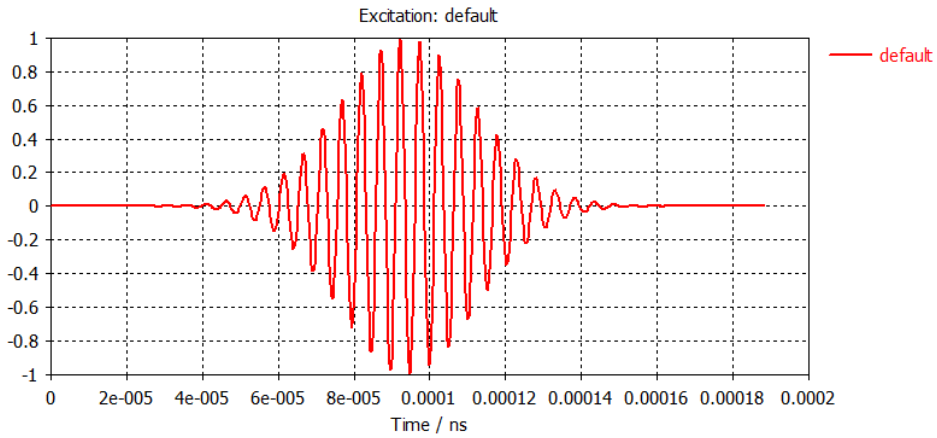

Fig. 5.6: Excitation signal

5.2.6 Post Processing:

Right after the simulation the post processing allow us to get the transmittance, reflectance, absorbance curves along with the field distribution pattern.

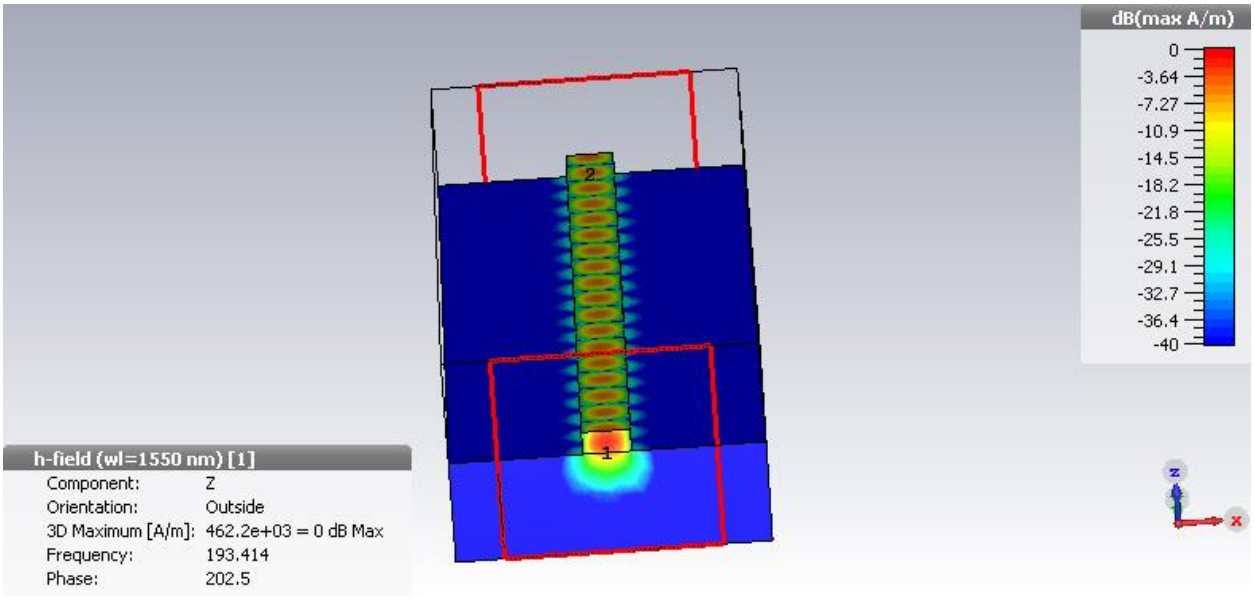

Fig. 5.7: Hz field distribution of single mode waveguide

As waveguide has been designed for single mode from Fig. 5.7 it is cleared that the only a mode is fitting to the propagation direction.

Chapter 6

Tesla type valve and its waveguide analogue

6.1 Introduction to Tesla-type Valve

Tesla valve is a fixed-geometry passive check valve. It allows a fluid to flow in one direction, without moving parts. The device is named after Nikola Tesla, who was awarded a patent in 1920 for its invention. This chapter is going to describe the working principle of basic tesla type valve and the correspondences between electromagnetic wave theory and shallow water theory. Based on our discussion at the end of this chapter a tesla type optical diode will be proposed. And implant that proposed device in the nonreciprocal system which will be discussed in the next chapter.

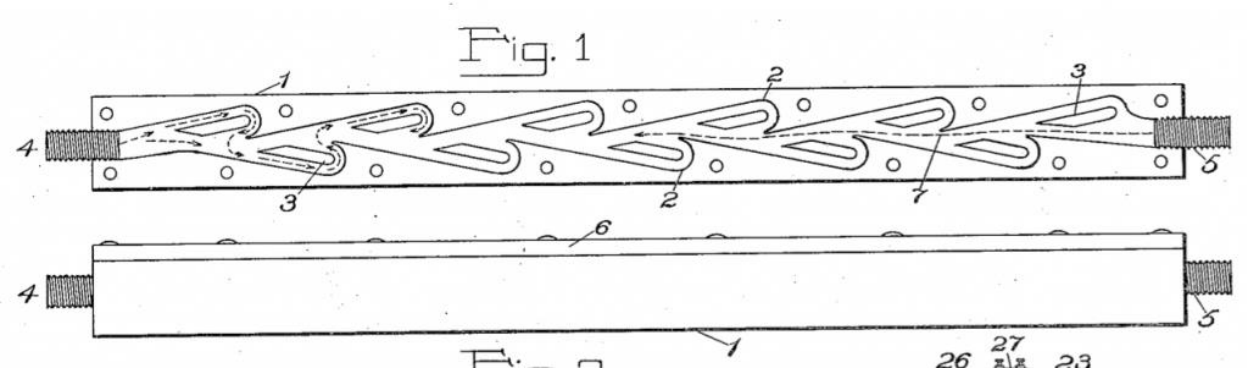

Fig. 6.1: Tesla valve design proposed by tesla[94]

6.2 Diodicity Mechanism of Tesla-type Micro Valves

The geometry of Tesla micro valve is shown in Fig 6.2. It is consisted of six regions 1) inlet channel, 2) main channel, 3) side-channel, 4) T-junction, 5) Y-junction and 6) outlet channel. In the case of forward flow, the fluid is accelerated at the entrance of fluid from goblet-shaped plenum to the channel and velocity gradient is created. While, the flow is developing, it reaches

into the T-junction. Some of the flow is drawn into the side-channel and a small jet is formed along the guide vane in the side channel. Here, 85% of the main channel fully developed flow continues to

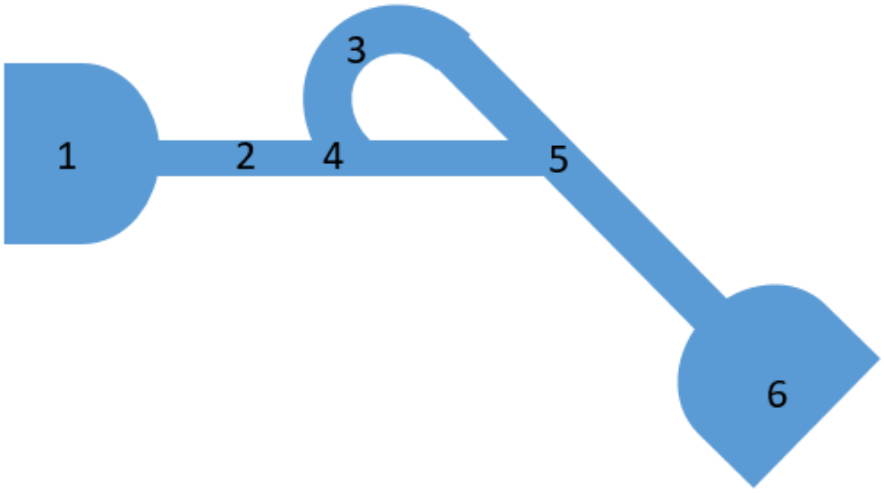

Fig. 6.2: Basic Tesla valve

route without any disturbance. In reverse flow the fluid right after the goblet-shaped plenum enters into the Y-junction and the flow is divided into two sections, one through the side-channel another through the main channel, similar type of jet is formed in both the channels. Then in the T-junction the two jets will counteract each other creating a huge disturbance there. Thus the reverse flow is restricted in the valve.

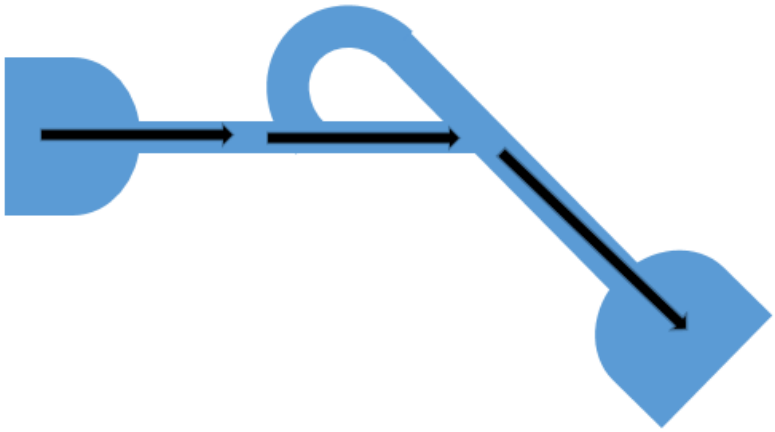

Fig. 6.3: Tesla valve Forward flow

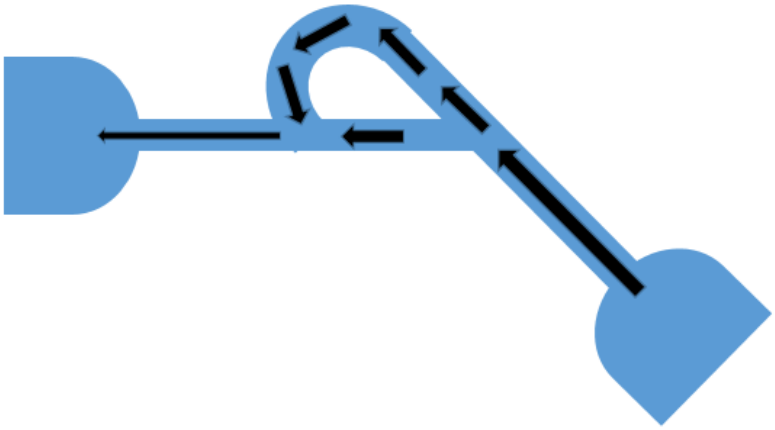

Fig. 6.4: Tesla valve Reverse flow

6.3 Correspondences between Electromagnetic Wave Theory and Shallow Water Theory

The quest for fluidic valve having non movable parts has a great impact on this research. Right after the findings of that valve the mathematical correspondence between SW wave and EM wave became a major task for this thesis. After discovering the mathematical correspondence a proof is needed either in hardware or in software. Here in this chapter the proof of the mathematical correspondence is provided using CST software. Thereby the mathematical correspondence has been bench-marked.

Although electromagnetic waves are different from waves in fluid, correlations can be drawn between the two. The common fluid waves can be longitudinal and transverse. Longitudinal waves move parallel to the direction of propagation and Transverse waves move perpendicular to the direction of propagation. Shallow water waves are characterized by transverse wave. Examination of shallow water wave theory reveals a strong analogy with EM wave since they are transverse.

Fig 6.5 describes a wave in SW theory. The mathematical modelling of SW theory has been obtained and can be summarized in this chapter[95]. Here a layer of fluid has been plotted in a coordinate system. h_B represents the bottom boundary indicating some height above a constant

absolute bottom. The surface has nominal distance H above the bottom. We have to restrict our universe to two dimensional in order to portrait shallow water phenomena.

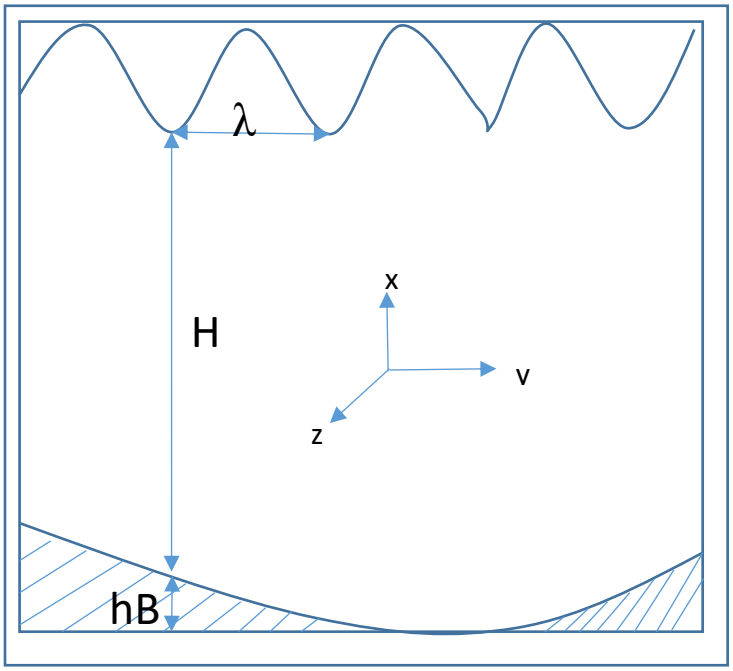

Fig. 6.5: Geometry of shallow water waves[95]

The Maxwell's equations in a source free region:

$$\nabla \times \boldsymbol{E} = -\frac{\partial \boldsymbol{B}}{\partial t} \tag{6.1}$$

$$\nabla \times \boldsymbol{E} = -\frac{\partial \boldsymbol{D}}{\partial t} \tag{6.2}$$

$$\nabla . \boldsymbol{D} = 0 \tag{6.3}$$

$$\nabla . \boldsymbol{B} = 0 \tag{6.4}$$

Here, *D=ε. E and B=μ. H*

The parameters ε and μ are complex tensor which depend on frequency. For simplification let us consider μ a scalar constant. Just like equation 3.14 (chapter 3) the magnetic field can be derived for time harmonic, two dimensional waves

$$\frac{\partial^2 \boldsymbol{H}}{\partial x^2} + \frac{\partial^2 \boldsymbol{H}}{\partial z^2} + (\omega^2 \mu \epsilon)\boldsymbol{H} = 0 \qquad (6.5)$$

The fundamental equation of motion for a fluid are based on conservation of mass, momentum and energy. The mathematical modelling of SW theory has been obtained and can be summarized below[95].

The velocities can be found as solutions to the following differential equations:

$$\left(\frac{\partial^2}{\partial t^2} + f^2\right)\boldsymbol{u} = -g\left(\frac{\partial^2 \eta}{\partial x \partial t} + f\frac{\partial \eta}{\partial y}\right) \qquad (6.6)$$

$$\left(\frac{\partial^2}{\partial t^2} + f^2\right)\boldsymbol{u} = -g\left(\frac{\partial^2 \eta}{\partial y \partial t} + f\frac{\partial \eta}{\partial x}\right) \qquad (6.7)$$

Where η is the height above the nominal value of the fluid depth, H_0, at a point allowing a time varying disturbance on the surface suggests defining $H(x,y,t)=H_0(x,y)+\eta(x,y,t)$

The equation for EM wave and SW waves can be written in a generalized form, assuming time harmonic waves:

$$\frac{\partial^2 \boldsymbol{\psi}}{\partial x^2} + \frac{\partial^2 \boldsymbol{\psi}}{\partial y^2} + iA_1\frac{\partial \boldsymbol{\psi}}{\partial x} + iA_2\frac{\partial \boldsymbol{\psi}}{\partial y} + A_3\boldsymbol{\psi} = 0 \qquad (6.21)$$

For Shallow water wave theory

$$A_1 = -\frac{f}{\omega H_0}\frac{\partial H_0}{\partial y}$$

$$A_2 = \frac{f}{\omega H_0}\frac{\partial H_0}{\partial x}$$

$$A_3 = \frac{\omega^2 - f^2}{C_0^2}$$

For electromagnetic wave theory,

$$A_1 = 0$$

$$A_2 = 0$$

$$A_3 = \frac{\omega^2 - \omega_p^2}{c^2}$$

So the velocity field in Shallow water wave theory and the magnetic field in EM wave theory are analogous to each other. To verify this phenomena one [96] Tesla type fluid valve has been chosen. The velocity field distribution is given there. A similar type structure has been modelled using CST in the electromagnetic domain. The magnetic field is then observed and compared with the fluid Valve's velocity field. The structure of the Tesla type valve has been shown in Figure 6.6

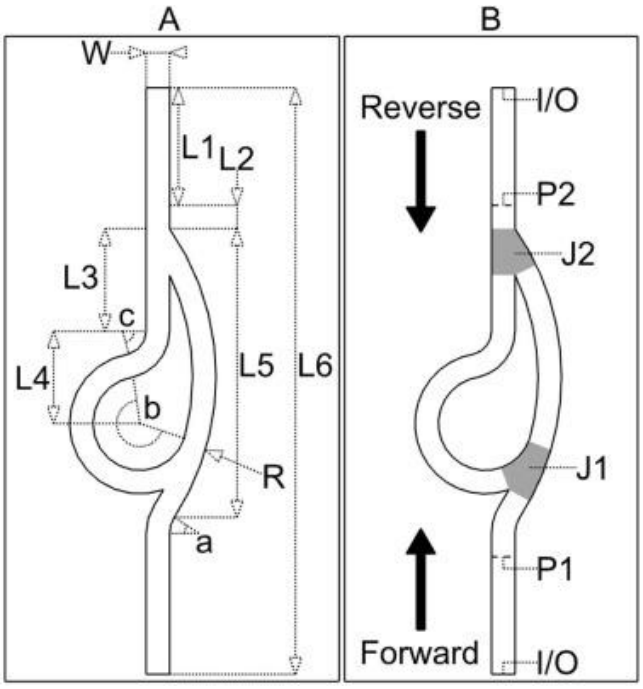

Fig. 6.6: Tesla type Valve structure[96]

The dimension of the structure[96] is given below in table -6.1

Table 6.1: Dimension of Tesla type fluidic valve

Parameter	Value in mm
W	2
L1	10
L2	2
L3	8.75
L4	7.85
L5	24.65
L6	50
R	22
a	2.5
b	4
c	2

In order to facilitate single mode propagation, the width of the waveguide is needed to be 0.445 μm. Let's assume W=.445 μm. The rest of the dimension is given in Table 6.2

Table 6.2: Deduced Dimension of Tesla type EM Diode

Parameter	Value in mm (fluid)	Value in μm (EM)
W	2	0.445
L1	10	2.22
L2	2	0.445
L3	8.75	1.95
L4	7.85	1.75
L5	24.65	5.48
L6	50	11.1125
R	22	4.895
a	2.5	0.55625
b	4	0.89
c	2	0.445

The velocity field and the magnetic field have been analyzed for Tesla type fluid valve and newly designed structure. Each of the structure has similar type flow pattern of wave for forward and reverse flow. This is perfectly observed in Figure 6.7. For the forward flow the both the

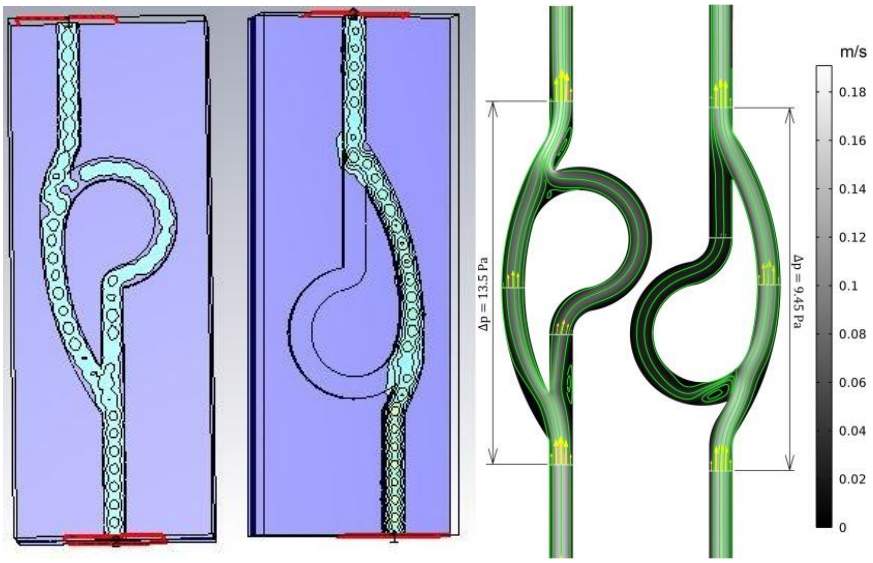

(a) (b)

Fig. 6.7: Similar type flow pattern of EM wave (a) and fluid wave [94] (b) in analogous structures

In Figure 6.7(a) the magnetic field of the deduced analogous structure has been shown whereas the Figure 6.7(b) shows the Velocity field distribution of the Tesla type fluid valve. The structures only main channel contributes to flow in the forward direction. But for reverse flow has been hindered by the main channel and side channel conjunction in the T-junction in both the structure. Thus it can be concluded that the Tesla type valve analogy can be used in Electromagnetics. However, with only single stage tesla type analogous diode reciprocity can't be broken. The S-parameter for both source to sink and sink to source are almost identical. This is because the design that have been chosen for the mechanical fluidic valve is itself doesn't produce higher isolation. The Diodicity that this mechanical valve has produced is around 1.4 times. However, the researchers have shown that the Diodicity increases with higher Reynolds number of the fluid.

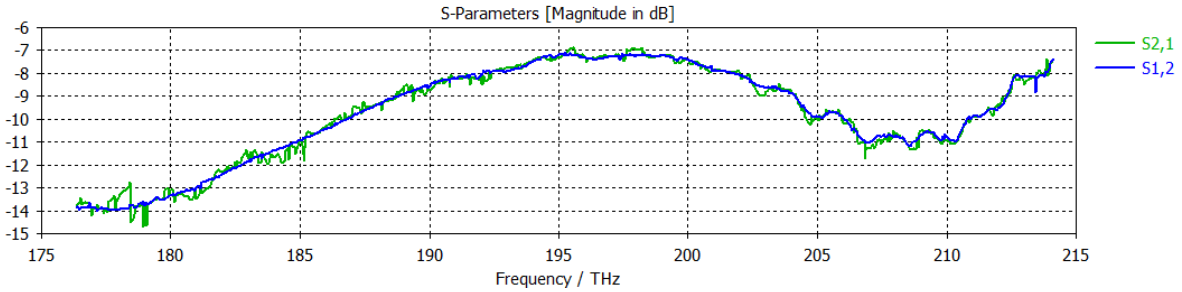

Fig. 6.8: S-parameter for both forward and backward propagation of a single stage tesla diode

Hence modification in the design is needed. In the next chapter the modification will be discussed.

Chapter 7

Proposed Structure, results and Discussion

In this chapter the proposed structure and the response of the optical nonreciprocal system have been discussed. The magnetic field distribution will be discussed and analyzed. The S-parameters for the forward propagation and backward propagation will be compared. The frequency response will also be analyzed to validate its application for the WDM systems. At the end of the chapter the footprint, working wavelength and isolation will be compared with some of the recently published SOI based Isolators.

7.1Proposed Optical Non-reciprocal System

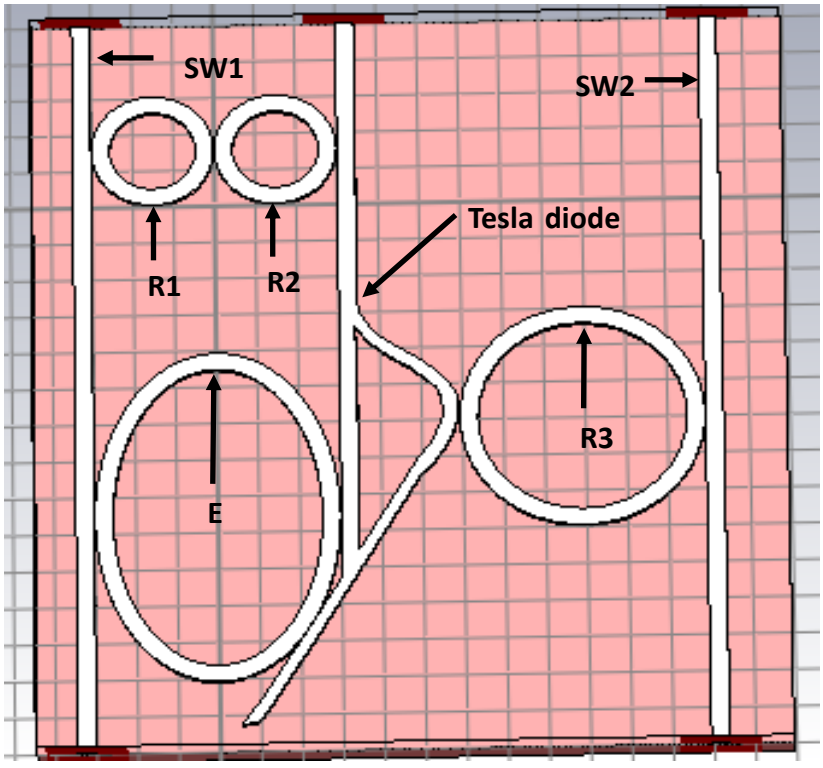

Fig. 7.1: Proposed nonreciprocal structure

Figure 7.1 describes the proposed structure. It consists of 3 ring waveguides R1, R2, and R3; two Straight Waveguides SW1 and SW2; one elliptical waveguide and a basic tesla diode.

The dimension of each of the component is given below in table -7.1

Table: 7.1: Proposed system's component dimension

Ring Structure				
Name	Outer Radius (μm)		Width (μm)	Height (μm)
R1	1.5		0.445	0.22
R2	1.5		0.445	0.22
R3	3		0.445	0.22
Elliptical structure				
Name	Major Radius(μm)	Minor Radius(μm)	Width (μm)	Height (μm)
E	4.5	3	0.445	0.22
Straight Waveguide				
Name	Length (μm)		Width (μm)	Height (μm)
SW1	20		0.445	0.22
SW2	20		0.445	0.22

The total footprint of the structure is 20 μm ×20 μm. The width and the height of the SOI waveguide is kept fixed to facilitate single mode propagation only to avoid multimode dispersion loss. The gap between the components are given in table-7.2

Table: 7.2: Proposed system's coupling gaps

Coupling components	Coupling Gap	Notion
SW1-R1	10nm	K1
R1-R2	10nm	K2
R2-TESLA DIODE(main channel)	10nm	K3
TESLA DIODE (Side channel)-R3	10nm	K4
SW1-E	10nm	K5
E- TESLA DIODE(main channel)	10nm	K6
E- TESLA DIODE(Y Junction channel)	<10nm	K7
R3-SW2	10nm	K8

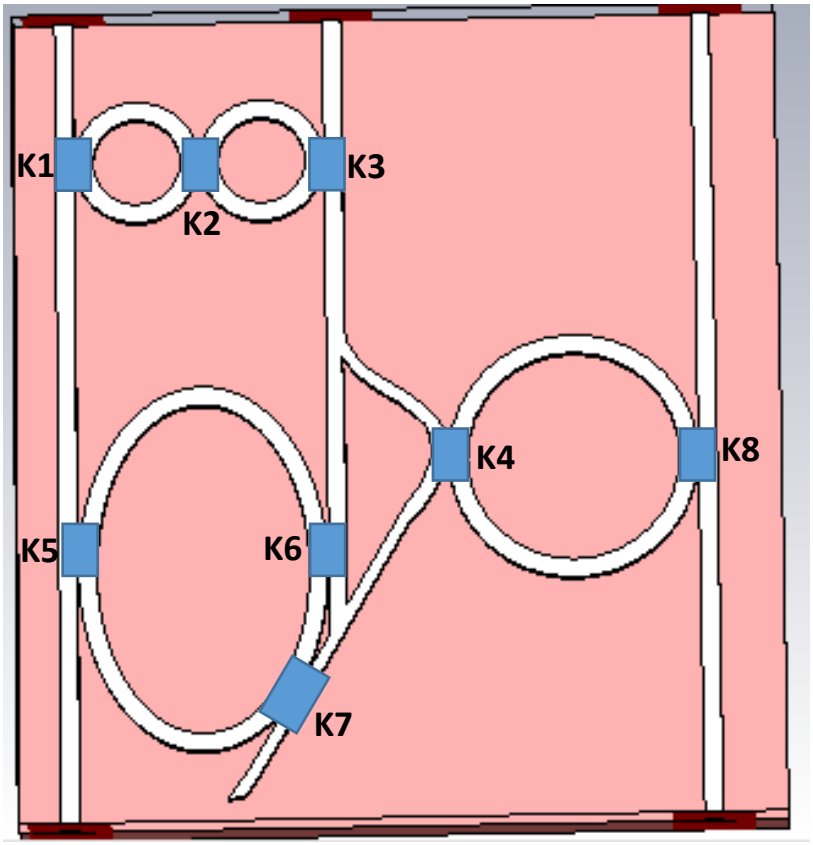

Fig. 7.2: Coupling gaps in the proposed nonreciprocal structure

7.2 Diodicity Mechanism of Proposed Structure

7.2.1 Forward Propagation

In figure 7.3 the path for the forward propagation has been shown. The input wave at first travels through SW2 to R3 via K8 coupling gap. Then from R3 it is passed to the side channel of TESLA diode via K4 coupling. Now the path is via coupling K3-K2-K1. The two coupling junctions are travelled by the wave at first from TESLA diode to R2 then From R2 to SW1. And the Wave is channeled out to output port through SW1.

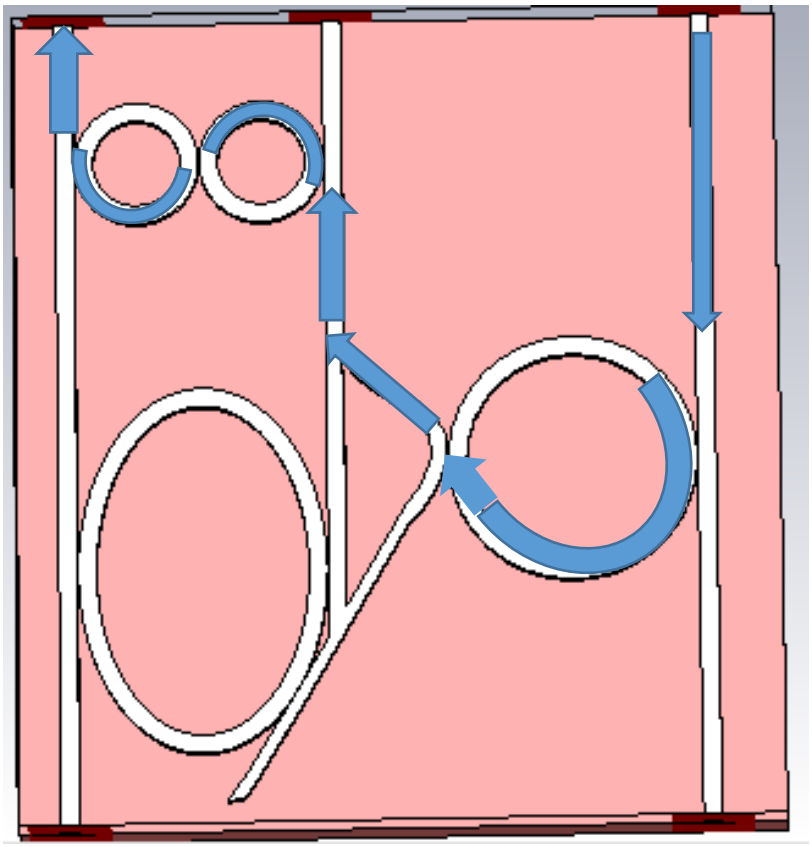

Fig. 7.3: Forward propagation

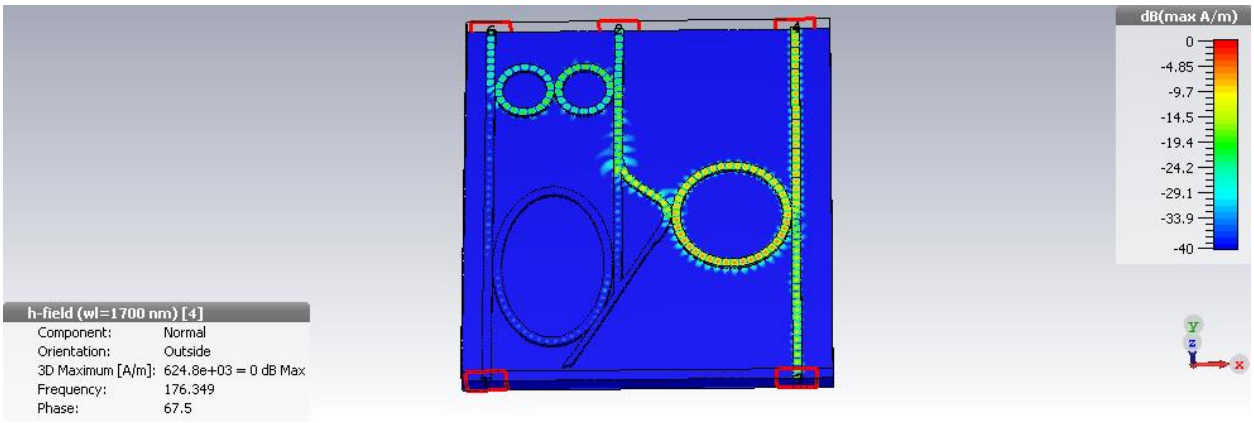

Fig. 7.4: Hz field for forward propagation

7.2.2 Backward Propagation

Here in the reverse operation the both R1, R2 and E transfer the input wave to the TESLA diode. The R1, R2 involve K1-K2-K3 and E involves K5, K6, and K7 to pass the input wave. As the coupling gap between E and Y-junction of the Tesla diode is less than 10 nm they have higher coupling. Thus the side channel of TESLA diode is dominated by the incoming wave from E-TESLA diode (K7). And via K4 and K8 this wave is transferred to SW2 through R3. Compared to the forward propagation the wave is transmitted to the SW2 but in reverse direction. Figure 7.5 and Figure 7.6 illustrates this phenomenon.

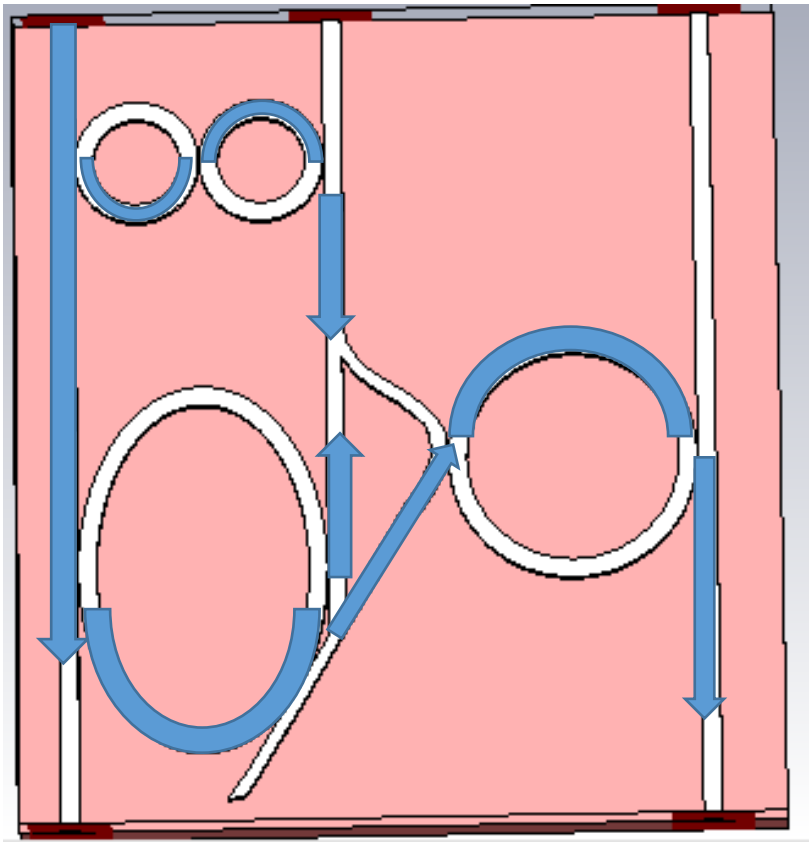

Fig. 7.5: Backward propagation

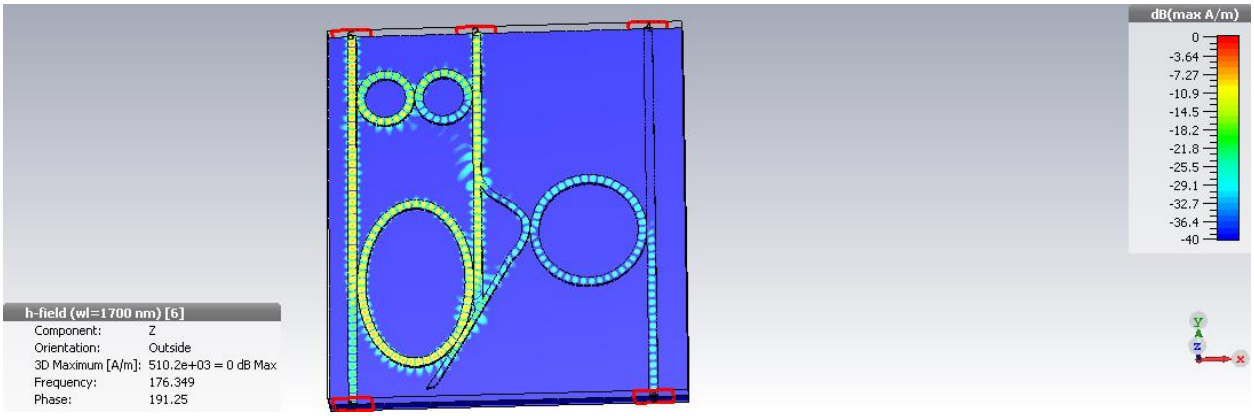

Fig. 7.6: Hz field for backward propagation

The impact of the Tesla diode can be better understood by replacing it with a normal straight waveguide in the proposed structure. Fig. 7.7 clearly shows that without Tesla type diode the proposed structure just acts like a simple Ring Resonator. In Fig. 7.7(a) the two adjacent waveguide along with the ring R3 depict the phenomena of Basic optical ring resonator. Figure 7.8 describes the performance of a simple Ring resonator. The Ring Resonator in Fig. 7.8 is become resonant at frequencies $\lambda 1$, λa. So from the input it will pass the $\lambda 1$ towards the drop port and rest of the frequencies will be passed to the throughput port. Moreover, as λa is a resonant frequency too. Hence from the throughput port it will be passed towards the add port. From Fig. 7.7(a) it is evident that the wave propagation in that particular structure is similar to that of the Fig. 7.8.

Form Fig. 7.7 (b) it is understood that the Tesla diode hinders the bidirectional flow unlike in Fig. 7.7 (a) and Fig. 7.8. Thereby the impact of Tesla type diode is understood.

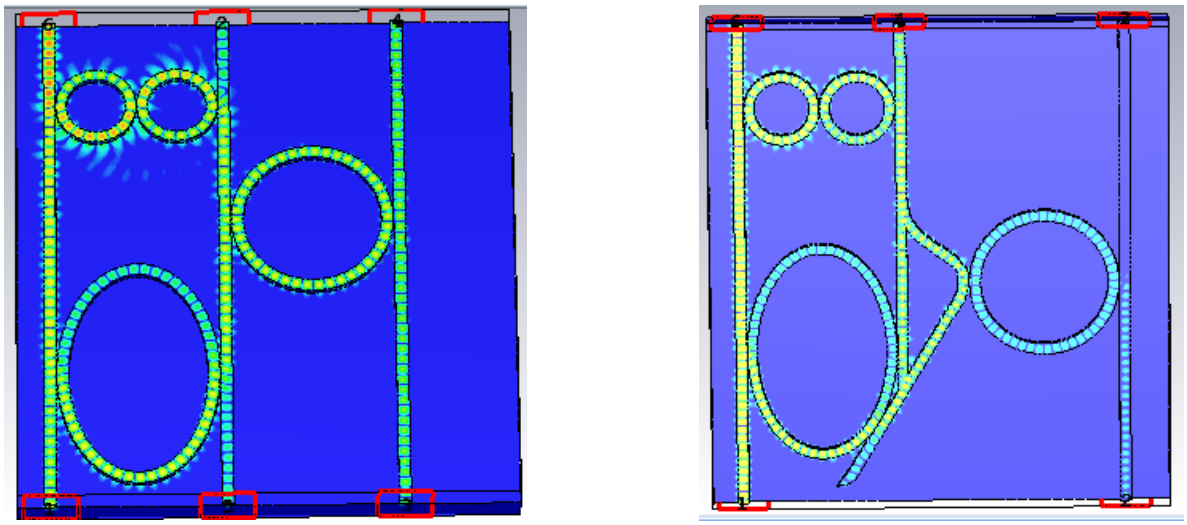

(a) (b)

Fig.7.7: Magnetic field, Hz propagation without Tesla type diode (a); with tesla type diode (b)

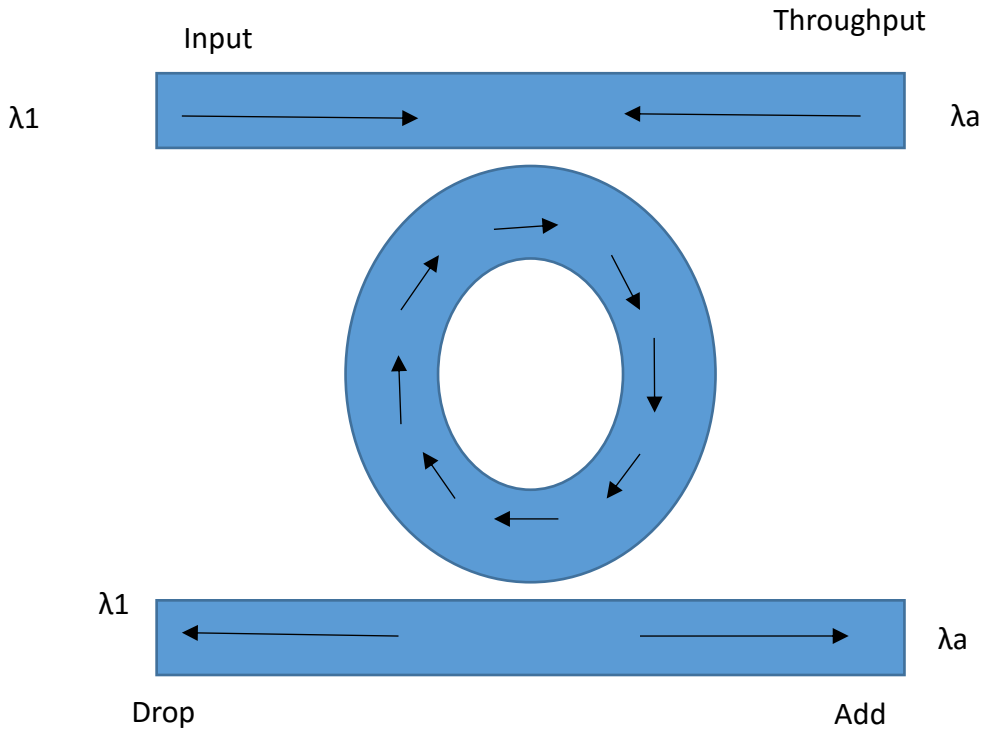

Fig. 7.8: Ring Resonator with two adjacent waveguide working Principle

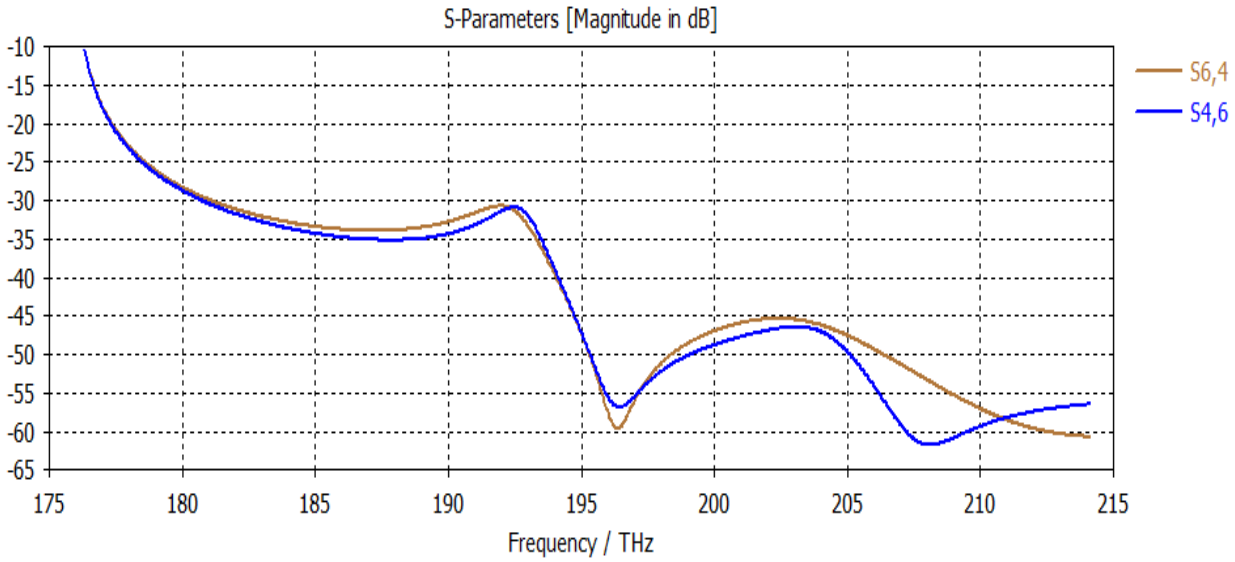

Fig 7.9: S-parameter for both forward and backward propagation without Tesla Diode

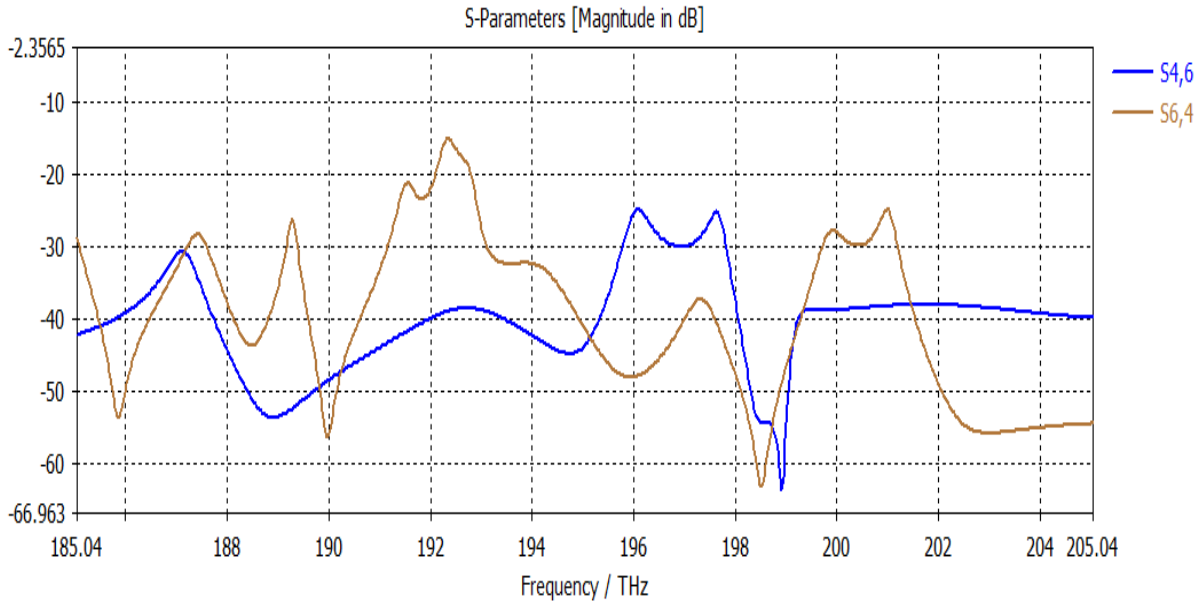

Fig 7.10: S-parameter for both forward and backward propagation with Tesla Diode

7.3 S-parameter Analysis

In CST S-parameter of the proposed design has been observed. Here for forward propagation the input port is port no.4 and the output port is port no.6. For the reverse operation the ports will be switched. Now by observing the S parameter the best isolation at WDM working wavelength.

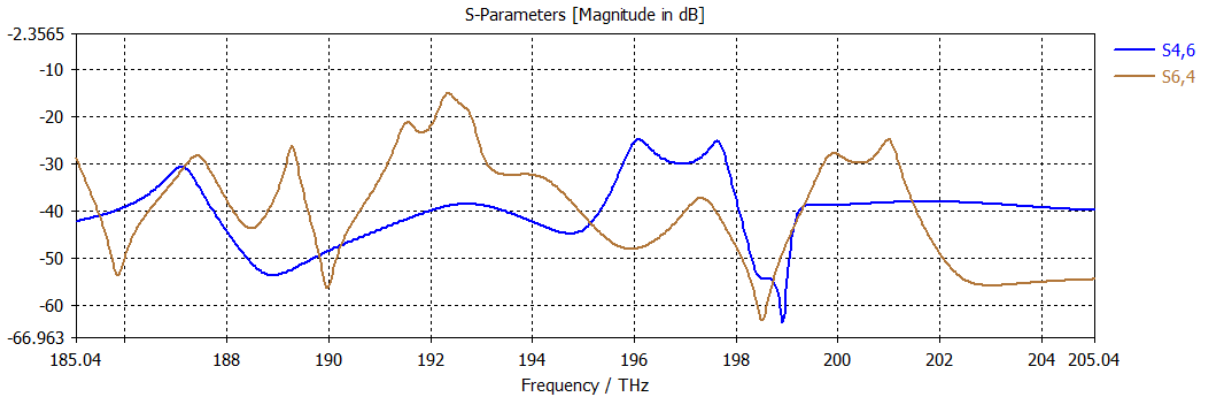

Fig 7.11: S-parameter for both forward and backward propagation

Wavelength division multiplexing systems can combine signals with multiplexing and split them apart with a demultiplexer. For that MUX-DEMUX operation optical isolation is needed. WDM systems are divided according to wavelength categories, generally course WDM (CWDM) and dense WDM (DWDM). CWDM operates with 8 channels (i.e., 8 fiber optic cables) in what is known as the C-Band with wavelengths about 1550 nm (≈194 THz). DWDM also operates in the C-Band but with 40 channels at 100 GHz spacing or 80 channels at 50 GHz spacing. The working wavelength for DWDM is between 1528 nm (≈191 THz) to 1563 nm (≈196 THz). At this window the maximum Isolation that our proposed device can provide is 24dB at 192.35 THz (≈1537 nm) Figure 7.8 depicts the scenario.

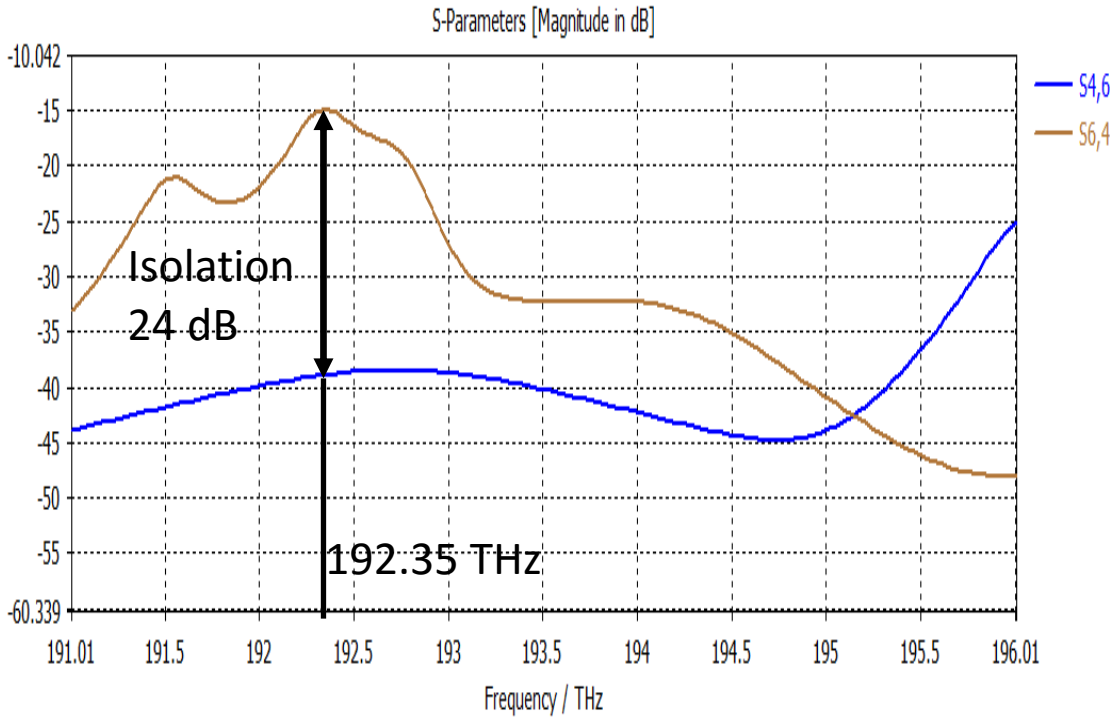

Fig. 7.12: Performance of the proposed design at DWDM working Frequency

Chapter 8

Conclusion and Future Scopes

8.1 Comparison with Existing SOI Based Isolators

Certainly the proposed structure has some outstanding features compared to the existing isolators. Firstly, the proposed optical nonreciprocal system is neither magnetically biased nor thermally biased, like the other isolators. So, the proposed structure can appear as a potential device for those scenario where external magnetic or thermal bias is deleterious for the device. Now a comparison with some of the recent isolator is provided in Table: 8.1

Table 8.1: Performance comparison with existing SOI based nonreciprocal system

Researcher	structure	Isolation	Length of the device	Working wavelength	Proposed design
T.Mizumoto 's group: Y.Shoji etc.[24]	MZI	>21 dB	NA	1530-1565 nm	3 dB higher isolation
T.Mizumoto 's group: Y.Shoji etc.[25]	MZI	21 dB	4 mm	1559 nm	3 dB higher isolation, smaller in size
T.Mizumoto 's group: Y.Shoji etc.[26]	MZI	18 dB	>1.5×1.5 mm^2	1322 nm	6 dB higher isolation, smaller in size
T.Mizumoto 's group: Y.Shoji etc.[27]	MZI	28 dB	>1.5×1.5 mm^2	1552 nm	4 dB lesser isolation, smaller in size
T.Mizumoto 's group: Y.Shoji etc.[15]	MZI	26.7 dB	>1.5×1.5 mm^2	1553 nm	2.7dB lesser isolation, smaller in size
John E.Bowers' group: MingChun Tien etc.[28]	Ring	9 dB	1.8 mm	1550 nm	15 dB higher isolation, smaller in size
John E.Bowers' group: D. Huang, P.Pintus and etc.[12]	Ring	32 dB	NA	1555nm	8 dB lesser isolation
Caroline A. Ross's Group: L. Bi etc.[10]	Ring	19.5 dB	290 μm	1550nm	3.5 dB higher isolation, smaller in size

Researcher	structure	Isolation	Length of the device	Working wavelength	Proposed design
Caroline A. Ross's Group: X. Sun etc.[11]	Ring	13±2.2 dB	NA	1564.4nm	~10 dB higher isolation
Roel Baets' group: S.Ghosh etc.[29]	MZI	25 dB	3.46×0.46 mm	1495.2 nm	1 dB lesser isolation, smaller in size
Roel Baets' group: S.Ghosh etc.[30]	MZI	11 dB	1.5 mm×4 μm	1512.6nm	13 dB higher isolation, smaller in size
Roel Baets' group: S.Ghosh etc.[13]	MZI	32 dB	6 mm×0.2mm	1540.5nm	8 dB lesser isolation, smaller in size
Mercedeh Khajavikhan [31]	Directional coupler	23 dB	NA	1555 nm	1 dB lesser isolation

From the above comparison Table it can be concluded that the proposed structure has better performance either in foot print or in isolation ratio. Besides it won't affect to any thermal or magnet dependencies. The proposed structure can be fabricated using CMOS technology which leads to cheap fabrication cost. And the operating frequency is within the WDM range. So it can be use for Optical fiber based Telecommunication applications. Last but not the least the design itself is a novel design. In this thesis, for designing the nonreciprocal system a correspondence between mechanical wave and Electromagnetic wave has been shown and then proved using simulation in CST.

8.2 Future Scopes

Based on this thesis some suggestions can be made about possible future scopes. Though the design is novel but there are still many issues which remain unsolved. Among them the following are listed as possibilities for future works.

- The tesla type structure can be used in other frequencies also. Using the similar structure nonreciprocity can be achieved in GHz range.

- Other than SOI, Lithium Niobate based waveguide can also be used. Then a performance comparison between these two can be done.
- Through in this research magnet less system has been considered. Moreover, using an external magnetic bias along with this structure isolation ration can be increased.
- Only single stage Tesla diode has been considered. Using multistage, series parallel combination of this novel structure higher isolation can be achieved.

References:

[1] (2019). *Cisco Visual Networking Index: Global Mobile Data Traffic Forecast Update, 2017–2022 White Paper*. Available: https://www.cisco.com/c/en/us/solutions/collateral/service-provider/visual-networking-index-vni/white-paper-c11-738429.html

[2] R. A. Paulus, "The Lorentz reciprocity theorem and range-dependent propagation modeling," *IEEE transactions on antennas and propagation*, vol. 42, pp. 270-272, 1994.

[3] K. Wapenaar, "Retrieving the elastodynamic Green's function of an arbitrary inhomogeneous medium by cross correlation," *Physical review letters*, vol. 93, p. 254301, 2004.

[4] L. Knopoff and A. F. Gangi, "Seismic reciprocity," *Geophysics*, vol. 24, pp. 681-691, 1959.

[5] Y. Yang, Z. Xu, L. Sheng, B. Wang, D. Xing, and D. Sheng, "Time-reversal-symmetry-broken quantum spin Hall effect," *Physical review letters*, vol. 107, p. 066602, 2011.

[6] H. Wang, H. Wu, and J.-q. Zhou, "Nonreciprocal optical properties based on magneto-optical materials: n-InAs, GaAs and HgCdTe," *Journal of Quantitative Spectroscopy and Radiative Transfer*, vol. 206, pp. 254-259, 2018.

[7] Y. Shoji, K. Miura, and T. Mizumoto, "Optical nonreciprocal devices based on magneto-optical phase shift in silicon photonics," *Journal of Optics*, vol. 18, p. 013001, 2015.

[8] T. Mizumoto, R. Baets, and J. E. Bowers, "Optical nonreciprocal devices for silicon photonics using wafer-bonded magneto-optical garnet materials," *MRS Bulletin*, vol. 43, pp. 419-424, 2018.

[9] J. Prat-Camps, P. Maurer, G. Kirchmair, and O. Romero-Isart, "Circumventing magnetostatic reciprocity: a diode for magnetic fields," *Physical review letters*, vol. 121, p. 213903, 2018.

[10] L. Bi, J. Hu, P. Jiang, D. H. Kim, G. F. Dionne, L. C. Kimerling, *et al.*, "On-chip optical isolation in monolithically integrated non-reciprocal optical resonators," *Nature Photonics*, vol. 5, p. 758, 2011.

[11] X. Y. Sun, Q. Du, T. Goto, M. C. Onbasli, D. H. Kim, N. M. Aimon, *et al.*, "Single-step deposition of cerium-substituted yttrium iron garnet for monolithic on-chip optical isolation," *Acs Photonics*, vol. 2, pp. 856-863, 2015.

[12] D. Huang, P. Pintus, C. Zhang, Y. Shoji, T. Mizumoto, and J. E. Bowers, "Electrically driven and thermally tunable integrated optical isolators for silicon photonics," *IEEE Journal of Selected Topics in Quantum Electronics*, vol. 22, pp. 271-278, 2016.

[13] S. Ghosh, S. Keyvaninia, Y. Shirato, T. Mizumoto, G. Roelkens, and R. Baets, "Optical isolator for TE polarized light realized by adhesive bonding of Ce: YIG on silicon-on-insulator waveguide circuits," *IEEE Photonics Journal*, vol. 5, pp. 6601108-6601108, 2013.

[14] Y. Shoji, A. Fujie, and T. Mizumoto, "Silicon waveguide optical isolator operating for TE mode input light," *IEEE Journal of Selected Topics in Quantum Electronics*, vol. 22, pp. 264-270, 2016.

[15] Y. Shoji, Y. Shirato, and T. Mizumoto, "Silicon Mach–Zehnder interferometer optical isolator having 8 nm bandwidth for over 20 dB isolation," *Japanese Journal of Applied Physics,* vol. 53, p. 022202, 2014.
[16] D. C. Hutchings, C. Zhang, B. M. Holmes, P. Dulal, A. D. Block, and B. J. Stadler, "Faraday polarisation mode conversion in semiconductor waveguides incorporating periodic garnet claddings," in *Integrated Optics: Devices, Materials, and Technologies XX*, 2016, p. 97500V.
[17] B. J. Stadler and T. Mizumoto, "Integrated magneto-optical materials and isolators: a review," *IEEE Photonics Journal,* vol. 6, pp. 1-15, 2014.
[18] H. Tu and Y. Xu, "A silicon-on-insulator complementary-metal-oxide-semiconductor compatible flexible electronics technology," *Applied Physics Letters,* vol. 101, p. 052106, 2012.
[19] M. Nur-E-Alam, M. Vasiliev, V. Kotov, and K. Alameh, "Recent developments in magneto-optic garnet-type thin-film materials synthesis," *Procedia Engineering,* vol. 76, pp. 61-73, 2014.
[20] M. C. Onbasli, L. Beran, M. Zahradník, M. Kučera, R. Antoš, J. Mistrík, *et al.*, "Optical and magneto-optical behavior of cerium yttrium iron garnet thin films at wavelengths of 200–1770 nm," *Scientific reports,* vol. 6, p. 23640, 2016.
[21] T. Haider, "A Review of Magneto-Optic Effects and Its Application," *International Journal of Electromagnetics and Applications,* vol. 7, pp. 17-24, 2017.
[22] Y. Shoji and T. Mizumoto, "Magneto-optical non-reciprocal devices in silicon photonics," *Science and technology of advanced materials,* vol. 15, p. 014602, 2014.
[23] X.-W. Xu, L. Song, Q. Zheng, Z. Wang, and Y. Li, "Optomechanically induced nonreciprocity in a three-mode optomechanical system," *Physical Review A,* vol. 98, p. 063845, 2018.
[24] Y. Shoji, I.-W. Hsieh, R. M. Osgood, and T. Mizumoto, "Polarization-independent magneto-optical waveguide isolator using TM-mode nonreciprocal phase shift," *Journal of Lightwave Technology,* vol. 25, pp. 3108-3113, 2007.
[25] Y. Shoji, T. Mizumoto, H. Yokoi, I.-W. Hsieh, and R. M. Osgood Jr, "Magneto-optical isolator with silicon waveguides fabricated by direct bonding," *Applied physics letters,* vol. 92, p. 071117, 2008.
[26] Y. Shoji, M. Ito, Y. Shirato, and T. Mizumoto, "MZI optical isolator with Si-wire waveguides by surface-activated direct bonding," *Optics express,* vol. 20, pp. 18440-18448, 2012.
[27] Y. Shirato, Y. Shoji, and T. Mizumoto, "High isolation in silicon waveguide optical isolator employing nonreciprocal phase shift," in *Optical Fiber Communication Conference*, 2013, p. OTu2C. 5.
[28] M.-C. Tien, T. Mizumoto, P. Pintus, H. Kromer, and J. E. Bowers, "Silicon ring isolators with bonded nonreciprocal magneto-optic garnets," *Optics express,* vol. 19, pp. 11740-11745, 2011.
[29] S. Ghosh, S. Keyvavinia, W. Van Roy, T. Mizumoto, G. Roelkens, and R. Baets, "Ce: YIG/Silicon-on-Insulator waveguide optical isolator realized by adhesive bonding," *Optics express,* vol. 20, pp. 1839-1848, 2012.
[30] S. Ghosh, S. Keyvaninia, Y. Shoji, W. Van Roy, T. Mizumoto, G. Roelkens, *et al.*, "Compact Mach–Zehnder interferometer Ce: YIG/SOI optical isolators," *IEEE Photonics Technology Letters,* vol. 24, pp. 1653-1656, 2012.

[31] P. Aleahmad, M. Khajavikhan, D. Christodoulides, and P. LiKamWa, "Integrated multi-port circulators for unidirectional optical information transport," *Scientific reports*, vol. 7, p. 2129, 2017.
[32] L. Fan, J. Wang, L. T. Varghese, H. Shen, B. Niu, Y. Xuan, *et al.*, "An all-silicon passive optical diode," *Science*, vol. 335, pp. 447-450, 2012.
[33] M. Hafezi and P. Rabl, "Optomechanically induced non-reciprocity in microring resonators," *Optics express*, vol. 20, pp. 7672-7684, 2012.
[34] F. Ruesink, M.-A. Miri, A. Alu, and E. Verhagen, "Nonreciprocity and magnetic-free isolation based on optomechanical interactions," *Nature communications*, vol. 7, p. 13662, 2016.
[35] M.-A. Miri, F. Ruesink, E. Verhagen, and A. Alù, "Optical nonreciprocity based on optomechanical coupling," *Physical Review Applied*, vol. 7, p. 064014, 2017.
[36] D. H. Malz, "Periodic driving and nonreciprocity in cavity optomechanics," University of Cambridge, 2019.
[37] Z. Yu and S. Fan, "Complete optical isolation created by indirect interband photonic transitions," *Nature photonics*, vol. 3, p. 91, 2009.
[38] M. Yamaguchi and K. Nobusada, "Indirect interband transition induced by optical near fields with large wave numbers," *Physical Review B*, vol. 93, p. 195111, 2016.
[39] H. Lira, Z. Yu, S. Fan, and M. Lipson, "Electrically driven nonreciprocity induced by interband photonic transition on a silicon chip," *Physical review letters*, vol. 109, p. 033901, 2012.
[40] Y. Shi and S. Fan, "Dynamic non-reciprocal meta-surfaces with arbitrary phase reconfigurability based on photonic transition in meta-atoms," *Applied Physics Letters*, vol. 108, p. 021110, 2016.
[41] G. Chen, G. Zhou, and F. S. Chau, "One-Way Polarization Rotation by Indirect Interband Transitions," *IEEE Photonics Technology Letters*, vol. 28, pp. 1557-1560, 2016.
[42] X. Zang and C. Jiang, "Nonlinear dynamic properties of nonreciprocal indirect interband photonic transitions," *JOSA B*, vol. 26, pp. 2275-2279, 2009.
[43] H. Hodaei, M. A. Miri, A. U. Hassan, W. Hayenga, M. Heinrich, D. Christodoulides, *et al.*, "Parity-time-symmetric coupled microring lasers operating around an exceptional point," *Optics letters*, vol. 40, pp. 4955-4958, 2015.
[44] L. Feng, Z. J. Wong, R.-M. Ma, Y. Wang, and X. Zhang, "Single-mode laser by parity-time symmetry breaking," *Science*, vol. 346, pp. 972-975, 2014.
[45] J. Ren, Y. G. Liu, M. Parto, W. E. Hayenga, M. P. Hokmabadi, D. N. Christodoulides, *et al.*, "Unidirectional light emission in PT-symmetric microring lasers," *Optics express*, vol. 26, pp. 27153-27160, 2018.
[46] I. H. Giden, K. Dadashi, M. Botey, R. Herrero, K. Staliunas, and H. Kurt, "Asymmetric light transmission in PT-symmetric microring resonators," *IEEE Journal of Selected Topics in Quantum Electronics*, vol. 22, pp. 19-24, 2016.
[47] P. Chamorro-Posada, "Gap solitons and symmetry breaking in parity-time symmetric microring coupled resonator optical waveguides," *JOSA B*, vol. 31, pp. 2728-2735, 2014.
[48] Y. Shi, Z. Yu, and S. Fan, "Limitations of nonlinear optical isolators due to dynamic reciprocity," *Nature photonics*, vol. 9, p. 388, 2015.
[49] S. Hua, J. Wen, X. Jiang, Q. Hua, L. Jiang, and M. Xiao, "Demonstration of a chip-based nonlinear optical isolator," *arXiv preprint arXiv:1606.04400*, 2016.

[50] Y. Choi, C. Hahn, J. W. Yoon, S. H. Song, and P. Berini, "Extremely broadband, on-chip optical nonreciprocity enabled by mimicking nonlinear anti-adiabatic quantum jumps near exceptional points," *Nature communications,* vol. 8, p. 14154, 2017.
[51] M. C. Hoffmann, N. C. Brandt, H. Y. Hwang, K.-L. Yeh, and K. A. Nelson, "Terahertz kerr effect," *Applied Physics Letters,* vol. 95, p. 231105, 2009.
[52] E. Freysz and J. Degert, "Nonlinear optics: terahertz Kerr effect," *Nature photonics,* vol. 4, p. 131, 2010.
[53] M. E. Yousif, "The Faraday Effect Explained."
[54] W. Chen, D. Leykam, Y. D. Chong, and L. Yang, "Nonreciprocity in synthetic photonic materials with nonlinearity," *MRS Bulletin,* vol. 43, pp. 443-451, 2018.
[55] S. Longhi, "Stopping and time reversal of light in dynamic photonic structures via Bloch oscillations," *Physical Review E,* vol. 75, p. 026606, 2007.
[56] T. J. Kippenberg and K. J. Vahala, "Cavity opto-mechanics," *Optics express,* vol. 15, pp. 17172-17205, 2007.
[57] I. Favero and K. Karrai, "Optomechanics of deformable optical cavities," *Nature Photonics,* vol. 3, p. 201, 2009.
[58] D. Van Thourhout and J. Roels, "Optomechanical device actuation through the optical gradient force," *Nature Photonics,* vol. 4, p. 211, 2010.
[59] J. Ma and M. L. Povinelli, "Applications of optomechanical effects for on-chip manipulation of light signals," *Current Opinion in Solid State and Materials Science,* vol. 16, pp. 82-90, 2012.
[60] M. Metcalfe, "Applications of cavity optomechanics," *Applied Physics Reviews,* vol. 1, p. 031105, 2014.
[61] W. Pernice, M. Li, and H. Tang, "A mechanical Kerr effect in deformable photonic media," *Applied Physics Letters,* vol. 95, p. 123507, 2009.
[62] W. H. P. Pernice, M. Li, and H. Tang, "Theoretical investigation of the transverse optical force between a silicon nanowire waveguide and a substrate," *Optics express,* vol. 17, pp. 1806-1816, 2009.
[63] M. Li, W. Pernice, and H. Tang, "Tunable bipolar optical interactions between guided lightwaves," *Nature Photonics,* vol. 3, p. 464, 2009.
[64] J. Roels, I. De Vlaminck, L. Lagae, B. Maes, D. Van Thourhout, and R. Baets, "Tunable optical forces between nanophotonic waveguides," *Nature nanotechnology,* vol. 4, p. 510, 2009.
[65] A. Butsch, C. Conti, F. Biancalana, and P. S. J. Russell, "Optomechanical self-channeling of light in a suspended planar dual-nanoweb waveguide," *Physical review letters,* vol. 108, p. 093903, 2012.
[66] C. Conti, A. Butsch, F. Biancalana, and P. S. J. Russell, "Dynamics of optomechanical spatial solitons in dual-nanoweb structures," *Physical Review A,* vol. 86, p. 013830, 2012.
[67] P. T. Rakich, M. A. Popović, M. Soljačić, and E. P. Ippen, "Trapping, corralling and spectral bonding of optical resonances through optically induced potentials," *Nature Photonics,* vol. 1, p. 658, 2007.
[68] G. S. Wiederhecker, L. Chen, A. Gondarenko, and M. Lipson, "Controlling photonic structures using optical forces," *Nature,* vol. 462, p. 633, 2009.
[69] J. Rosenberg, Q. Lin, and O. Painter, "Static and dynamic wavelength routing via the gradient optical force," *Nature Photonics,* vol. 3, p. 478, 2009.

[70] M. L. Povinelli, S. G. Johnson, M. Lončar, M. Ibanescu, E. J. Smythe, F. Capasso, *et al.*, "High-Q enhancement of attractive and repulsive optical forces between coupled whispering-gallery-mode resonators," *Optics express,* vol. 13, pp. 8286-8295, 2005.
[71] T. Carmon and K. J. Vahala, "Modal spectroscopy of optoexcited vibrations of a micron-scale on-chip resonator at greater than 1 GHz frequency," *Physical review letters,* vol. 98, p. 123901, 2007.
[72] G. Anetsberger, R. Rivière, A. Schliesser, O. Arcizet, and T. J. Kippenberg, "Ultralow-dissipation optomechanical resonators on a chip," *Nature Photonics,* vol. 2, p. 627, 2008.
[73] G. Anetsberger, O. Arcizet, Q. P. Unterreithmeier, R. Rivière, A. Schliesser, E. M. Weig, *et al.*, "Near-field cavity optomechanics with nanomechanical oscillators," *Nature Physics,* vol. 5, p. 909, 2009.
[74] S. Weis, R. Rivière, S. Deléglise, E. Gavartin, O. Arcizet, A. Schliesser, *et al.*, "Optomechanically induced transparency," *Science,* vol. 330, pp. 1520-1523, 2010.
[75] E. Verhagen, S. Deléglise, S. Weis, A. Schliesser, and T. J. Kippenberg, "Quantum-coherent coupling of a mechanical oscillator to an optical cavity mode," *Nature,* vol. 482, p. 63, 2012.
[76] M. Eichenfield, C. P. Michael, R. Perahia, and O. Painter, "Actuation of micro-optomechanical systems via cavity-enhanced optical dipole forces," *Nature Photonics,* vol. 1, p. 416, 2007.
[77] M. Eichenfield, R. Camacho, J. Chan, K. J. Vahala, and O. Painter, "A picogram-and nanometre-scale photonic-crystal optomechanical cavity," *Nature,* vol. 459, p. 550, 2009.
[78] M. Eichenfield, J. Chan, R. M. Camacho, K. J. Vahala, and O. Painter, "Optomechanical crystals," *Nature,* vol. 462, p. 78, 2009.
[79] A. H. Safavi-Naeini, T. M. Alegre, J. Chan, M. Eichenfield, M. Winger, Q. Lin, *et al.*, "Electromagnetically induced transparency and slow light with optomechanics," *Nature,* vol. 472, p. 69, 2011.
[80] J. Chan, T. M. Alegre, A. H. Safavi-Naeini, J. T. Hill, A. Krause, S. Gröblacher, *et al.*, "Laser cooling of a nanomechanical oscillator into its quantum ground state," *Nature,* vol. 478, p. 89, 2011.
[81] M. Notomi, H. Taniyama, S. Mitsugi, and E. Kuramochi, "Optomechanical wavelength and energy conversion in high-Q double-layer cavities of photonic crystal slabs," *Physical review letters,* vol. 97, p. 023903, 2006.
[82] CST-Computer Simulation Technology [Online]. Available: https://www.cst.com/
[83] G. G. Stokes, *On the perfect blackness of the central spot in Newton's rings, and on the verification of Fresnel's formulae for the intensities of reflected and refracted rays,* 1849.
[84] C. Caloz, A. Alù, S. Tretyakov, D. Sounas, K. Achouri, and Z.-L. Deck-Léger, "Electromagnetic nonreciprocity," *Physical Review Applied,* vol. 10, p. 047001, 2018.
[85] J. Strutt, "Some general theorems relating to vibrations," *Proceedings of the London Mathematical Society,* vol. 1, pp. 357-368, 1871.
[86] A. T. de Hoop, "A reciprocity theorem for the electromagnetic field scattered by an obstacle," *Applied Scientific Research, Section B,* vol. 8, pp. 135-140, 1960.
[87] G. Afanasiev, "Simplest sources of electromagnetic fields as a tool for testing the reciprocity-like theorems," *Journal of Physics D: Applied Physics,* vol. 34, p. 539, 2001.
[88] L. D. Landau, J. Bell, M. Kearsley, L. Pitaevskii, E. Lifshitz, and J. Sykes, *Electrodynamics of continuous media* vol. 8: elsevier, 2013.

[89] M. Born and E. Wolf, "Principle of Optics7th edn," ed: Cambridge: Cambridge University Press, 1999.
[90] G. T. Reed and A. P. Knights, *Silicon photonics: an introduction*: John Wiley & Sons, 2004.
[91] J. F. Lotspeich, "Explicit general eigenvalue solutions for dielectric slab waveguides," *Applied optics*, vol. 14, pp. 327-335, 1975.
[92] A. Yariv, "Critical coupling and its control in optical waveguide-ring resonator systems," *IEEE Photonics Technology Letters*, vol. 14, pp. 483-485, 2002.
[93] D. G. Rabus, *Integrated ring resonators*: Springer, 2007.
[94] T. Nikola, "Valvular conduit," ed: Google Patents, 1920.
[95] P. E. J. D. G. Long, "CORRESPONDENCES BETWEEN ELECTROMAGNETIC WAVE THEORY AND SHALLOW WATER THEORY."
[96] S. de Vries, D. Florea, F. Homburg, and A. Frijns, "Design and operation of a Tesla-type valve for pulsating heat pipes," *International Journal of Heat and Mass Transfer*, vol. 105, pp. 1-11, 2017.